European Journal of Medicinal Chemistry 215 (2021) 113281

Contents lists available at ScienceDirect

European Journal of Medicinal Chemistry

journal homepage: http://www.elsevier.com/locate/ejmech

Design, synthesis, and biological evaluation of 4-benzoylamino-1H-pyrazole-3-carboxamide derivatives as potent CDK2 inhibitors

Tingting Lin [a, b, c, d], Jiacheng Li [b, d], Liping Liu [b, d], Yuanqing Li [b, d], Hualiang Jiang [a, b, d], Kaixian Chen [a, b, d], Pan Xu [b, *], Cheng Luo [a, b, d, **], Bing Zhou [c, d, ***]

[a] Shanghai Institute for Advanced Immunochemical Studies, and School of Life Science and Technology, ShanghaiTech University, Shanghai, 200031, China
[b] The Center for Chemical Biology, Drug Discovery and Design Center, State Key Laboratory of Drug Research, Shanghai Institute of Materia Medica, Chinese Academy of Sciences, 555 Zuchongzhi Road, Shanghai, 201203, China
[c] Department of Medicinal Chemistry, State Key Laboratory of Drug Research, Shanghai Institute of Materia Medica, Chinese Academy of Sciences, 555 Zuchongzhi Road, Shanghai, 201203, China
[d] University of Chinese Academy of Sciences, 19 Yuquan Road, Beijing, 100049, China

ARTICLE INFO

Article history:
Received 4 December 2020
Received in revised form
27 January 2021
Accepted 3 February 2021
Available online 11 February 2021

Keywords:
CDK2 inhibitor
Selectivity
Anti-proliferative potency

ABSTRACT

Cyclin-dependent kinases play significant roles in cell cycle progression and are promising targets for cancer therapy. However, most potent CDK inhibitors lack the balance between efficacy and safety because of poor selectivity. Given the roles of CDK2 in tumorigenesis, selective CDK2 inhibition may provide therapeutic benefits against certain cancer. In this study, a series of 4-benzoylamino-1H-pyrazole-3-carboxamide derivatives were designed, synthesized, and evaluated. The most selective compound **DC-K2in212** in this series exhibited high potency towards CDK2 and had effective anti-proliferative activity against A2058 melanoma cell line and MV4-11 leukemia cell line while exhibiting low toxic effect on human normal cell lines MRC5 and LX2. The molecular modeling illustrated that compound **DC-K2in212** had the similar binding mode with CDK2 as **C-73**, the most selective CDK2 inhibitor reported so far, which might account for selectivity against CDK2 over CDK1. Further biological studies revealed that compound **DC-K2in212** suppressed CDK2-associated downstream signaling pathway, blocked cell cycle progression, and induced cellular apoptosis. Therefore, compound **DC-K2in212** could serve as a potential CDK2 inhibitor for further development.

© 2021 Elsevier Masson SAS. All rights reserved.

1. Introduction

Cyclin dependent kinases (CDKs) are serine/threonine protein kinases that play significant roles in cell proliferation, apoptosis and transcription [1]. There are 20 CDKs in human cells which can be divided into two subfamilies represented as cell cycle-related family (e.g. CDK1-6) and transcription-related family (e.g. CDK7-13) according to their biological function [2]. The kinase activity of CDKs is tightly regulated by its cyclin regulatory partners and inhibitory proteins (CKIs).

As an important member of CDK family, CDK2 plays a critical role in regulating cell cycle progression. CDK2-cyclin E is involved in late G1 to make the full phosphorylation of retinoblastoma (Rb) to initiate S phase of cell cycle, whereas CDK2-cyclin A facilitates S/G2 transition. Besides, CDK2 also plays a role in adaptive immune response, apoptosis, cell differentiation, and normal DNA repair [3–6]. CDK2 and its regulatory proteins are responsible for loss of proliferation control, which might lead to cancer. For example, CDK2 is highly expressed in glioblastoma, melanoma, and lymphoid tumor tissues (Fig. S1), while its active regulator cyclin E is frequently overexpressed in various cancer cells, and inhibitory regulators p21 and p27 are often silenced during tumor progression [7–9]. CDK2 is also a critical factor involved in metastasis of prostate cancer [10], and inhibition of CDK2 could suppress proliferation of ovarian cancer cells with amplified CCNE1 expression [11], induce apoptosis of MYCN-amplified neuroblastoma cells [12], and

* Corresponding author.
** Corresponding author. Shanghai Institute for Advanced Immunochemical Studies, and School of Life Science and Technology, ShanghaiTech University, Shanghai, 200031, China.
*** Corresponding author. Department of Medicinal Chemistry, State Key Laboratory of Drug Research, Shanghai Institute of Materia Medica, Chinese Academy of Sciences, 555 Zuchongzhi Road, Shanghai, 201203, China.
E-mail addresses: xupan_322@simm.ac.cn, xvpan_322@simm.ac.cn (P. Xu), cluo@simm.ac.cn (C. Luo), zhoubing@simm.ac.cn (B. Zhou).

https://doi.org/10.1016/j.ejmech.2021.113281
0223-5234/© 2021 Elsevier Masson SAS. All rights reserved.

Abbreviations

CDK	cyclin-dependent kinase
CKI	cyclin-dependent kinase inhibitor
Rb	retinoblastoma protein
PI3K	phosphatidylinositol-3-kinase
BDR4	bromodomain-containing protein 4
SSphos	sodium 2'-(dicyclohexylphosphanyl)-2,6-dimethoxy-[1,1′-biphenyl]-3-sulfonate hydrate
EDCI	1-ethyl-(3-dimethylaminopropyl)carbodiimide hydrochiloride
HOBt	1-Hydroxybenzotriazole
Mcl-1	myeloid leukemia cell differentiation protein
PI	propidium iodide
PARP	poly ADP-ribose polymerase

cause the death of BRCA1-deficient cancers [6]. Moreover, the combination of CDK2 and phosphatidylinositol-3-kinase (PI3K) inhibitors could induce cell death in colorectal cancer while dual inhibition of CDK2 and bromodomain-containing protein 4 (BRD4) could cause apoptosis in MYC-amplified medulloblastoma cells [13,14]. Furthermore, inhibition of CDK2 might reverse acquired resistance of CDK4/6 inhibitors [15]. Overall, the above studies all suggest that CDK2 is a promising drug target for cancer therapy.

Over the past decades, a large number of CDK inhibitors with various scaffolds have been discovered (Fig. 1). Most of them are ATP-competitive inhibitors, which occupy the catalytic ATP binding site. Flavopiridol is the first pan-CDK inhibitor entered in clinical trials as a therapy for leukemia, breast cancer, colorectal cancer, gastric cancer and etc., which inhibits CDKs and other protein kinases [16,17]. Ongoing studies identified more selective CDK inhibitors and some have entered into clinical studies, such as Seliciclib [18], Dinaciclib [19,20], AT7519 [21,22], BAY-1000394 [23,24], PHA-848125 [25,26] and etc [27,28]. However, most of them lack the balance between efficacy and safety because of poor selectivity, which might hinder further development. So far, three selective CDK4/6 inhibitors (Palbociclib [29], Abemaciclib [30], and Ribociclib [31]) have been approved by U.S. Food and Drug Administration (FDA) for treatment of breast cancer, highlighting the importance of selectivity in developing CDK inhibitor. However, the most selective CDK2 inhibitor **C-73** having been reported so far had almost no anti-proliferative activity against cancer cells [32,33]. Therefore, improving selectivity of CDK inhibitors towards CDK2 with anti-proliferative activity remains an ongoing issue.

In this study, we chose a pan-CDK inhibitor AT7519 which is in phase I clinical study of lymphocytic leukemia therapy as a starting scaffold to design selective CDK2 inhibitors. AT7519 could effectively inhibit kinase activity of CDK1, CDK2 and CDK9, and show high anti-proliferation effect against various tumor cell lines, while it also affects the viability of normal cell line MRC-5 with high potency [34]. In order to optimize its selectivity towards CDK2, a series of 4-benzoylamino-1H-pyrazole-3-carboxamide derivatives were designed and synthesized as CDK2 inhibitors.

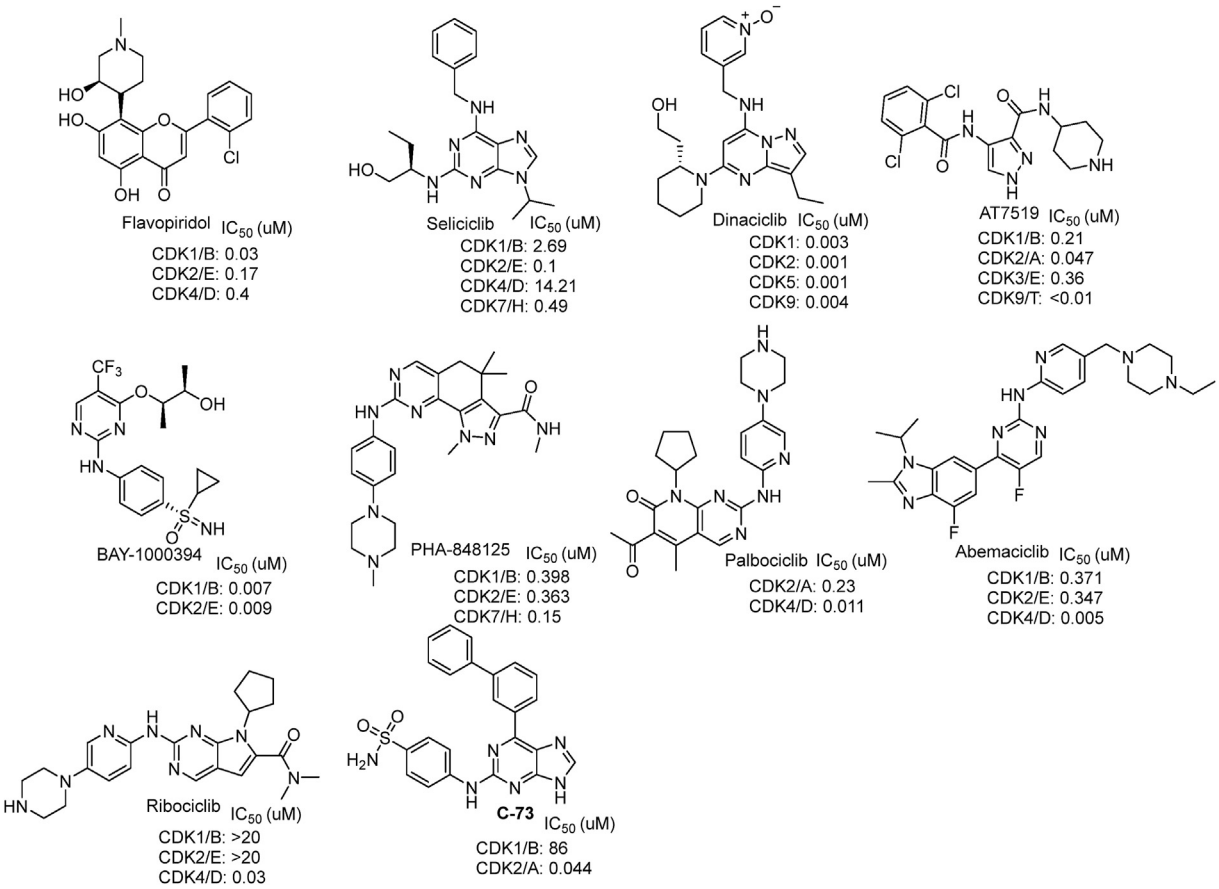

Fig. 1. Chemical structures of representative CDK inhibitors.

2. Results and discussion

2.1. Drug design and cchemistry

Inspired by the discovery of selective CDK2 inhibitor **C-73** [32], we aligned AT7519 to the complex structure of CDK2-**C-73**. As shown in Fig. 2, the 1H-pyrazole-3-carboxamide skeleton of AT7519 forms three hydrogen bonds with the hinge region of CDK2 (residue Glu81 and Leu83) and the whole molecule occupies the normal ATP binding site which is similar with **C-73**. Notably, the piperidine of AT7519 overlaps with the sulfamoylphenyl part of **C-73**. However, the 2, 6-dichlorophenyl of AT7519 shows a different structure orientation with purine-proximal phenyl ring of **C-73**, and AT7519 also lacks a group similar to the distal phenyl ring of **C-73** which might promote selectivity.

Based on the structural information, exploration of the region which is occupied by distal phenyl ring of **C-73** could be a feasible way to improve selectivity of AT7519 against CDK2. The 3-postion in phenyl of AT7519 is closer to the above-mentioned region, thus introducing groups at that position might help improve selectivity towards CDK2. Moreover, fluorine has lower steric hindrance relative to chlorine, which might make phenyl of AT7519 easier to rotate to the similar conformation as purine-proximal phenyl ring of **C-73**. However, the replacement of AT7519's chlorine with fluorine reduced the potency, while replacing piperidine with 4-fluorophenyl at the same time increased the potency against CDK2 (see Table 1). Compared to piperidine, the more rigid 4-fluorophenyl may promote and stabilize the 1H-pyrazole-3-carboxamide skeleton of compound anchoring to hinge region, which may further lead to improved binding affinity with CDK2 protein and higher potency of compounds. Based on these considerations, **DC-K2in2** therefore represented a reasonable starting point for further structure optimization.

The synthesis schemes of compounds are depicted in Scheme 1, amide coupling of 4-nitro-1H-pyrazole-3-carboxylic acid with corresponding amines provided compounds (**2**, **5**), followed by reduction of nitro with Pd/C, then acylation of compounds (**3**, **6**) with corresponding acids gave compounds (**4**, **7** and **DC-K2in2**). Compound **4** was deprotected with 2 M HCl in dioxane to obtain compound **DC-K2in1**. Compound **7** reacted with corresponding boric acid or pinacol ester, catalyzed by [Pd (ally)Cl]$_2$ and phosphorous ligand SSphos to give compounds (**DC-K2in201** - **DC-Kin209**, **8**, and **9a-9c**). Compound **8** was hydrolyzed by NaOH in

Table 1
Enzymatic activity and *in vitro* anti-proliferative activity evaluated in melanoma cell line A2058.

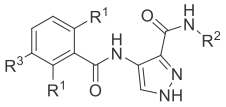

Compd.	R^1	R^2	R^3	IC_{50} (μM)		
				CDK1/cyclinB1	CDK2/cyclinA2	A2058
C-73	–	–	–	>200	0.543	>100
AT7519	Cl		H	0.089	0.032	0.166
DC-K2in1	F		H	0.594	0.250	NT
DC-K2in2	F		H	0.014	0.006	1.011
DC-K2in201	F			0.306	0.040	2.938
DC-K2in202	F			0.432	0.086	2.371

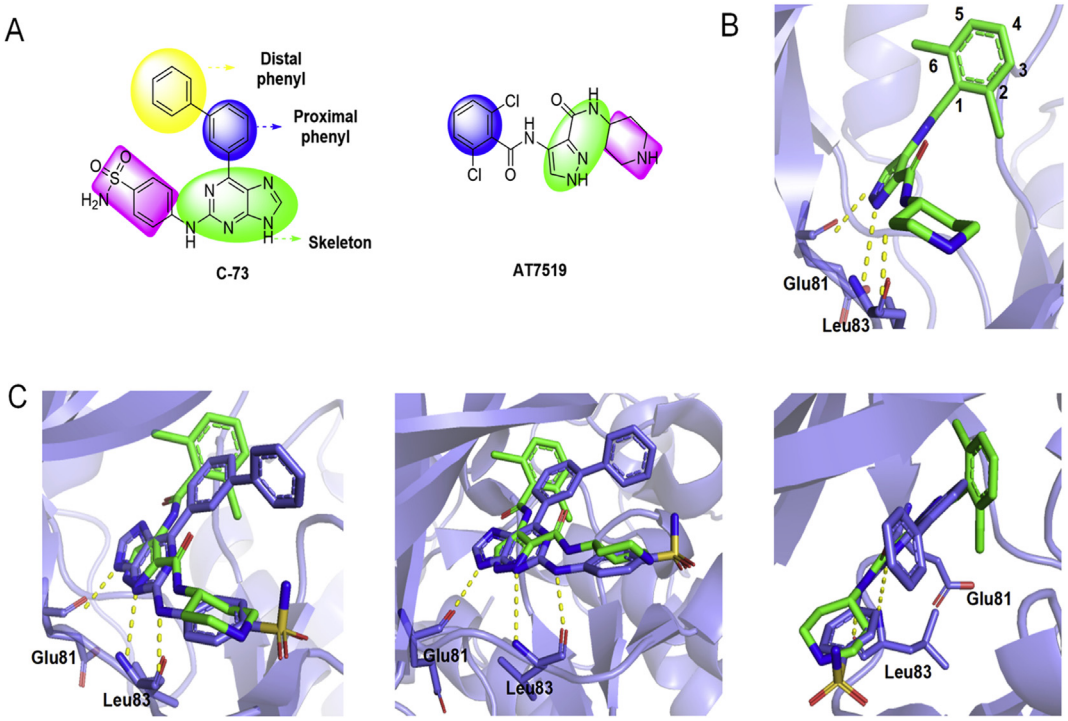

Fig. 2. Comparison of the binding mode between AT7519 and **C-73** within CDK2. Key residues of CDK2 are labeled, and hydrogen bonds in all panels are depicted by yellow dotted lines. (A) Structure of **C-73** and AT7519. (B) The binding mode of AT7519 in CDK2 (PDB code: 2VU3). (C) Alignment of AT7519 (green stick model) and **C-73** (purple stick model) within CDK2 (PDB code: 5NEV).

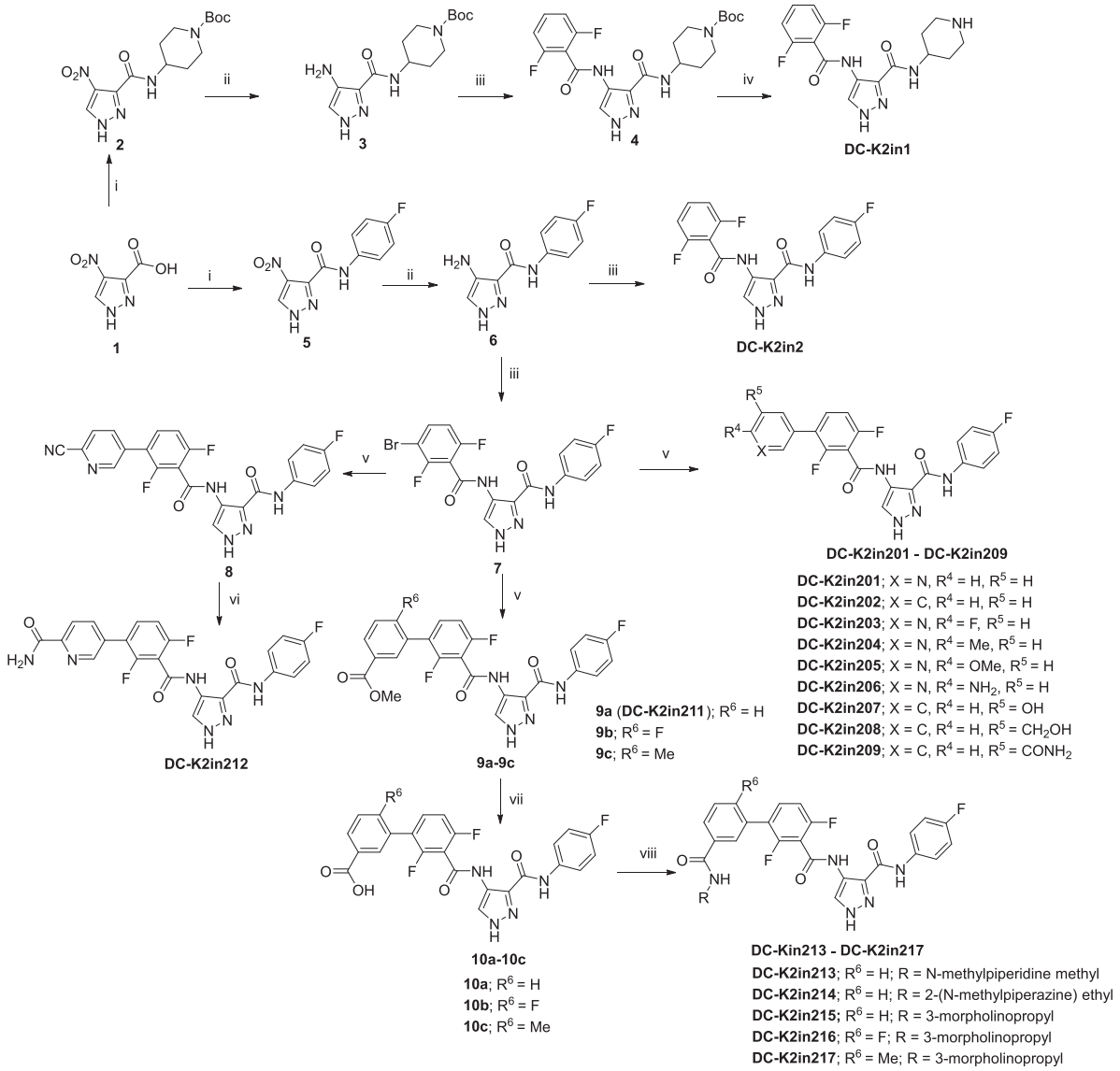

Scheme 1. [a]Reagents and conditions: (i) Corresponding amine, EDCI, HOBt, DMF, r.t., 2h; (ii) Pd/C, MeOH: THF = 3 : 1, H_2, 40 °C, 36h; (iii) Corresponding acid, EDCI, HOBt, DMF, rt, 2h; (iv) 2 M HCl in dioxane, r.t., DCM; (v) Corresponding boric acid or boric acid ester, [Pd (ally)Cl]$_2$, SSphos, K_3PO_4, 1,4-dioxane: H_2O = 3 : 1, 100 °C, 8h; (vi) NaOH, MeOH: H_2O = 1 : 1, 60 °C, 2h; (vii) LiOH·H_2O, MeOH: H_2O = 1 : 1, 40 °C, 4h; (viii) Corresponding amine, EDCI, HOBt, DMF, r.t., 18h.

mixture of water and methanol at 60 °C to give compound **DC-K2in212**. Compounds (**10a-10c**) was obtained from **10a-10c** by hydrolysis, then reacted with corresponding amines to give compounds (**DC-K2in213** – **DC-K2in217**).

2.2. Structure-activity relationships (SARs)

At the beginning of our research, compound **DC-K2in201** and **DC-K2in202**, which contained pyridyl or phenyl at 3-position on phenyl of compound **DC-K2in2** were synthesized to validate our design strategy. The kinase inhibition activity of compounds against CDK1/cyclinB1 and CDK2/cyclinA2 was tested *in vitro*. CDK2 is highly expressed in melanoma cell lines. Moreover, it is reported that in cells that are deficient in functional Rb but not p16^{INK4A}, cell cycle progression might dependent more on CDK2-mediated phosphorylation of RBL2 [35], thus the anti-proliferative activity of these compounds were evaluated in melanoma cell line A2058 in which Rb protein is absent because of nonsense mutation of *RB1* gene while p16^{INK4A} is still functional. As shown in Table 1, compounds **DC-K2in201** and **DC-K2in202** were more potent than **C-73** with IC_{50} of 40 nM and 86 nM against CDK2 while having higher selectivity than AT7519 and **DC-K2in2**, which was consistent with our expectation. Besides, compounds **DC-K2in201** and **DC-K2in202** exhibited a bit lower anti-proliferative activity relative to AT7519 with IC_{50} values of around 2 μM. Thus, further optimization was performed based on **DC-K2in201** and **DC-K2in202**.

According to the U-type conformation of **C-73** in complex with CDK2, we tried to modify the ortho-, meta- or para-postion in pyridyl or phenyl of compound **DC-K2in201** or **DC-K2in202** to produce the similar conformation as **C-73**. First, we introduced different groups at R^4 in pyridyl of **DC-K2in201** or R^5 in phenyl of **DC-K2in202**. As show in Table 2, compared with **DC-K2in201**, **DC-K2in203** which had fluorine at R^4 displayed similar potency in *in vitro* enzymatic inhibition assay but the cellular activity dropped slightly. Compounds (**DC-K2in204** – **DC-K2in206**) containing electron-donating groups (methyl, methoxyl, and amino) at R^4 reduced the potency against CDK1 and CDK2. Notably, **DC-K2in212** with electron-withdraw group carbamoyl exhibited 17-fold

Table 2
Enzymatic activity and *in vitro* anti-proliferative activity evaluated in melanoma cell line A2058.

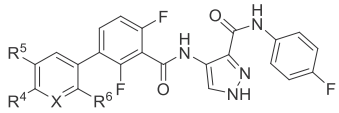

Compd.	X	R^4	R^5	R^6	IC_{50} (μM)		
					CDK1/cycinB1	CDK2/cyclinA2	A2058
DC-K2in201	N	H	H	H	0.306	0.040	2.938
DC-K2in203	N	F	H	H	0.278	0.051	6.308
DC-K2in204	N	Me	H	H	1.850	0.164	NT
DC-K2in205	N	OMe	H	H	0.712	0.144	NT
DC-K2in206	N	NH_2	H	H	1.262	0.120	8.540
DC-K2in212	N	$CONH_2$	H	H	1.019	0.058	0.295
DC-K2in202	C	H	H	H	0.432	0.086	2.371
DC-K2in207	C	H	OH	H	0.236	0.026	NT
DC-K2in208	C	H	CH_2OH	H	0.537	0.076	NT
DC-K2in211	C	H	COOMe	H	0.496	0.210	NT
DC-K2in209	C	H	$CONH_2$	H	0.069	0.008	1.989
DC-K2in213	C	H		H	0.743	0.082	3.340
DC-K2in214	C	H	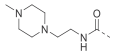	H	0.350	0.067	NT
DC-K2in215	C	H	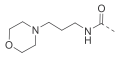	H	0.723	0.073	0.650
DC-K2in216	C	H	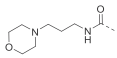	F	1.299	0.169	0.943
DC-K2in217	C	H	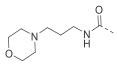	Me	3.689	0.485	6.514

NT (not test).

selectivity against CDK2 over CDK1 while showing effective anti-proliferative activity in A2058 cell line with IC_{50} value of 0.295 μM. As for R^5 substituents in phenyl of compound **DC-K2in202**, the inhibition activity of carbamoyl (**DC-K2in209**) substitution was more potent than any other substitutions including hydroxyl (**DC-K2in207**), hydroxymethyl (**DC-K2in208**), and methoxy formyl (**DC-K2in211**) when evaluated in *vitro* enzymatic assay. **DC-K2in209** showed over 8-fold selectivity against CDK2 over CDK1, while showing moderate anti-proliferative activity in A2058 cell line with IC_{50} value of 1.989 μM. We then introduced N-methylpiperidine methyl, 2-(N-methylpiperazine) ethyl and 3-morpholinopropyl at amide of compound **DC-K2in209** to obtain compound **DC-K2in213** – **DC-K2in215**. The activity of three derivatives decreased, suggesting that large steric hindrance at R^5 position were not benefit for enzymatic activity of compounds and had little effect on the increase of selectivity. Interestingly, **DC-K2in215** showed relatively good anti-proliferative activity with IC_{50} value of 0.650 μM in A2058 cell line. We also added fluorine and methyl at R^6 in **DC-K2in215**, but it resulted in decreasing both enzymatic activity and selectivity which might suggest steric hindrance at that position. Therefore, compound **DC-K2in12** turned out to be optimal in terms of selectivity and cellular activity in this series.

2.3. CDKs selectivity of compound *DC-K2in212*

DC-K2in212 was then evaluated in a panel of structurally similar CDK kinases including CDK3/cyclinE1, CDK4/cyclinD3, CDK6/cyclin D3, CDK7/cyclin H/MAT1, CDK9/cyclin T1, and CDK12 wt/cyclin K.

Table 3
Inhibitory profile of AT7519 and **DC-K2in212** against different CDKs.

Kinase	AT7519 IC_{50} (nM)	DC-K2in212 IC_{50} (nM)
CDK1/cyclinB1	210[a], 89[b]	1019[b]
CDK2/cyclinA2	47[a],32[b]	58[b]
CDK3/cyclinE1	360[a]	113[b]
CDK4/cyclinD3	72[b]	3478[b]
CDK6/cyclin D3	170[a]	>18000[b]
CDK7/cyclin H/MAT1	2400[a]	>18000[b]
CDK9/cyclin T1	<10[a], 5[b]	1119[b]
CDK12 wt/cyclin K	NT	>18000[b]

NT (not test).
[a] Reported by Matthew S. Squires et al. [34].
[b] From this work.

As shown in Table 3, **DC-K2in212** inhibited CDK1, CDK4, CDK6, CDK7, CDK9, and CDK12 with IC_{50} values above 1 μM, and CDK3 with IC_{50} value of 113 nM. Thus, **DC-K2in212** was a potent CDK2 inhibitor with above 10-fold selectivity against CDK1, CDK4, CDK6, CDK7, CDK9, and CDK12, while having around 2-fold selectivity against CDK3.

2.4. Binding mechanism of *DC-K2in212* to CDK2

To better understand the mechanism of inhibition, we used molecular docking to analyze the binding mode of **DC-K2in212** with CDK2. The crystal structure of CDK2 in complex with **C-73** was selected for docking studies. As depicted in Fig. 3, **DC-K2in212** exhibited U-type conformation similar to that of **C-73** and

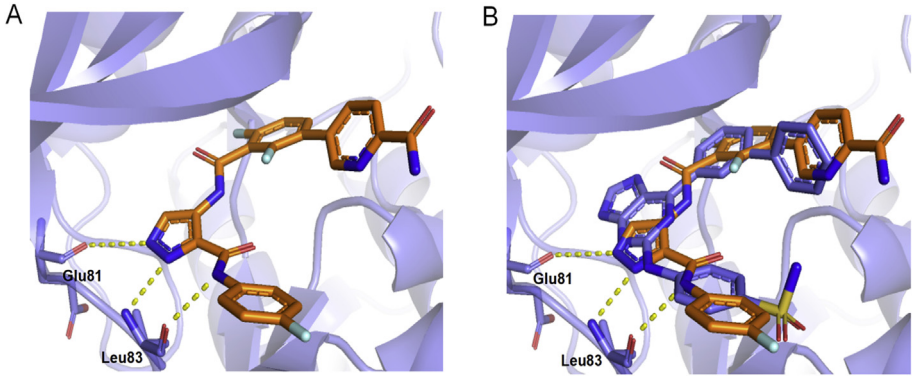

Fig. 3. Binding mode analysis of **DC-K2in212**. The key residues of CDK2 are labeled, and hydrogen bonds in all panels are depicted by yellow dotted lines. (A) Docking conformation of **DC-K2in212** (orange stick model) with CDK2. (B) Comparison of binding mode of **DC-K2in212** and **C-73** (purple stick model) within CDK2.

Table 4
In vitro anti-proliferative activity of AT7519 and **DC-K2in212** against cancer cells and normal cells.

Compd.	A2058 (IC_{50} μM)	MV4-11 (IC_{50} μM)	MRC5 (IC_{50} μM)	LX2 (Inhibition% at 100 μM)
AT7519	0.166	0.391	0.425	39.4
DC-K2in212	0.295	0.252	54.81	32.5

overlapped with **C-73** at the same region. The pyrazole ring formed three hydrogen bonds with Glu81 and Leu83 in hinge region of CDK2. 4-(6-carbamoyl-3-pyridyl)-2, 6-difluorophenyl emulates the position of biphenyl of **C-73**. The similar binding mode to **C-73** might account for the selectivity of **DC-K2in212**.

2.5. *In vitro anti-proliferative activity and toxicity evaluation of **DC-K2in212***

In acute myeloid leukemia, CDK2 inhibition leads to reactivation of differentiation pathway and arrest of tumor growth of AML [9]. Therefore, in addition to the human melanoma cell A2058, further cellular anti-proliferative activity of **DC-K2in212** was evaluated against human myeloid leukemia cell MV4-11, meanwhile human normal fibroblast cell MRC5 and human hepatic stellate cell LX2 were selected to evaluate toxicity of **DC-K2in212** (Table 4). **DC-K2in212** significantly inhibited A2058 and MV4-11 cells growth and displayed the similar high anti-proliferative activity as AT7519. Furthermore, **DC-K2in212** had lower toxic effect on human normal cell lines MRC5 and LX2 than AT7519, which might be caused by improved selectivity. Compared to AT7519, **DC-K2in212** had reduced activity against both CDK1 and CDK9 which played essential roles in normal cell cycle and transcriptional regulation, respectively [36]. This suggested that improved selectivity on CDK family members might alleviate toxicity.

2.6. *Effects of **DC-K2in212** on CDK2-associated signaling pathway*

To clarify effects of **DC-K2in212** on signaling pathway regulated by CDK2, Western blot analysis was used to detect the expression of proteins modulated by CDK2 after treatment with **DC-K2in212** at different concentrations in MV4-11 and A2058 cells. Rb is the phosphorylation target of CDK2 during late G1 phase, which is absence in A2058 cells as the result of nonsense mutation of *RB1*, so the level of phosphorylation of Rb was only detected in MV4-11 cells. As shown in Fig. 4A and B, treatment of **DC-K2in212** significantly inhibited Rb phosphorylation on Ser807/811 and Ser780 in a dose and time dependent way, suggesting potent on-target effects of **DC-K2in212** in cells. Given that Rb is phosphorylated by CDK4/6 and CDK2, the complete inhibition of Rb phosphorylation might need block on both CDK2 and CDK4/6. Therefore, treatment of **DC-K2in212** in low concentrations for 24 h exhibited mild inhibition on Rb phosphorylation, especially on Ser780, phosphorylated mainly by CDK4/6 [37]. Besides, previous study has indicated that CDK2 could regulate anti-apoptotic-related protein myeloid leukemia cell differentiation protein (Mcl-1) by phosphorylating to increase its stability [38]. Thus, the effects of **DC-K2in212** on Mcl-1 were analyzed. Treatment with **DC-K2in212** significantly downregulated Mcl-1 expression in A2058 and MV4-11 cells (Fig. 4C, **D**). Altogether, these results indicated that **DC-K2in212** could suppress CDK2-associated signaling pathways.

2.7. *Effects of **DC-K2in212** on cell cycle and apoptosis*

In order to detect the effect of **DC-K2in212** on cell cycle distribution, A2058 cells were stained with PI probes and subjected to flow cytometry analysis. As shown in Fig. 5A, treatment of A2058 cells with **DC-K2in212** at 0.2 μM induced accumulation of cells in S phase with a corresponding loss of cells in G1 phase, which was consistent with the effect of CDK2 knockdown using siRNA in A2058 cells (Fig. S2). Besides, the percentage of A2058 cells in S and G2/M phases were both increased at concentration up to 0.4 μM, which might be related to the function of CDK2 in DNA damage response, accumulation of DNA damage may lead to arrest in G2/M phase [6,39]. Overall, the data suggested that **DC-K2in212** might induce cell cycle arrest through different mechanisms.

CDK2 also regulates the process of cell apoptosis [4]. To determine the capacity of **DC-K2in212** in inducing cell apoptosis, after treating A2058 cells with **DC-K2in212**, Western blot and flow cytometry were used to analyze. Fig. 4D suggested that cleaved casepase-3 and cleaved PARP, two critical hallmarks of apoptosis, were noticeably up-regulated by the treatment with **DC-K2in212** in a dose-dependent manner. As shown in Fig. 5B, the total proportion of apoptotic cells were dependently increased from 9.72 to 68.6% with concentrations, revealing that **DC-K2in212** could induce cellular apoptosis in a dose-dependent manner.

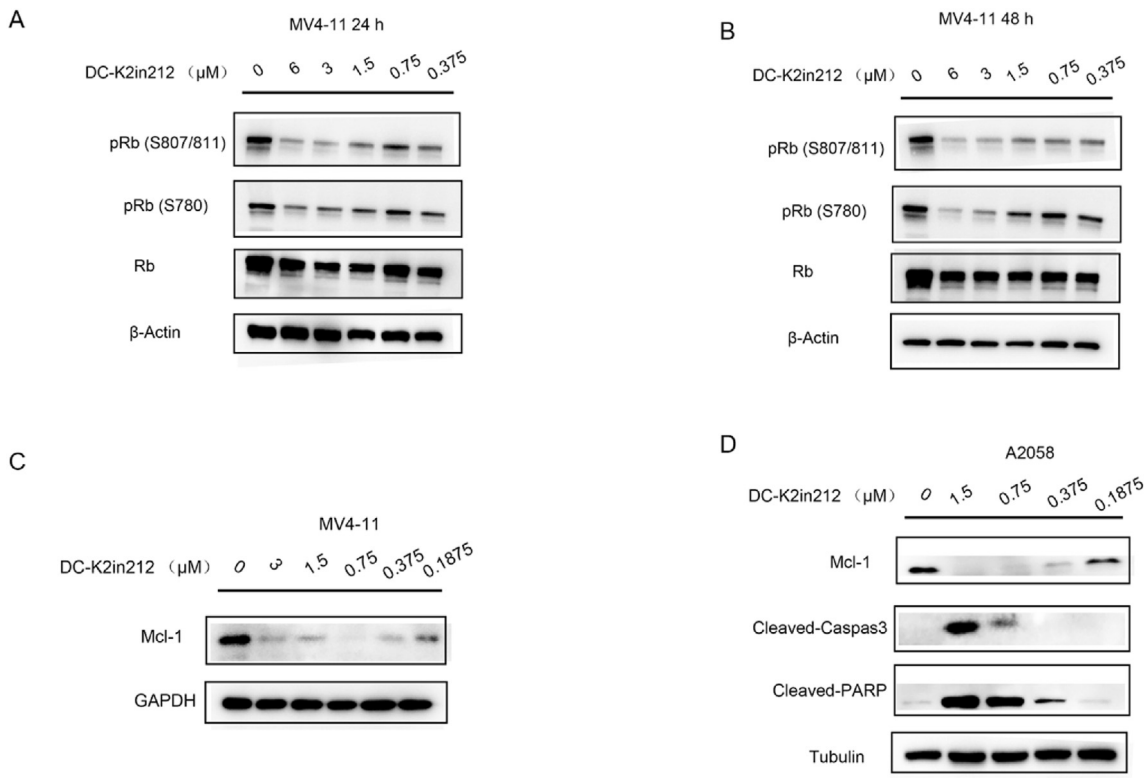

Fig. 4. **DC-K2in212** inhibits the function of CDK2. (A–B) **DC-K2in212** inhibits Rb phosphorylation. Immunoblot analysis of the indicated proteins in MV4-11 cells treated with **DC-K2in212** for 24 h (A) and 48 h (B). β-Actin was used as the loading control. (C) Immunoblot analysis of Mcl-1 protein in MV4-11 cells treated with **DC-K2in212** for 24 h, and GAPDH was used as a loading control. (D) Immunoblot analysis of the indicated proteins in A2058 cells treated with **DC-K2in212** for 24 h, and Tubulin was used as a loading control.

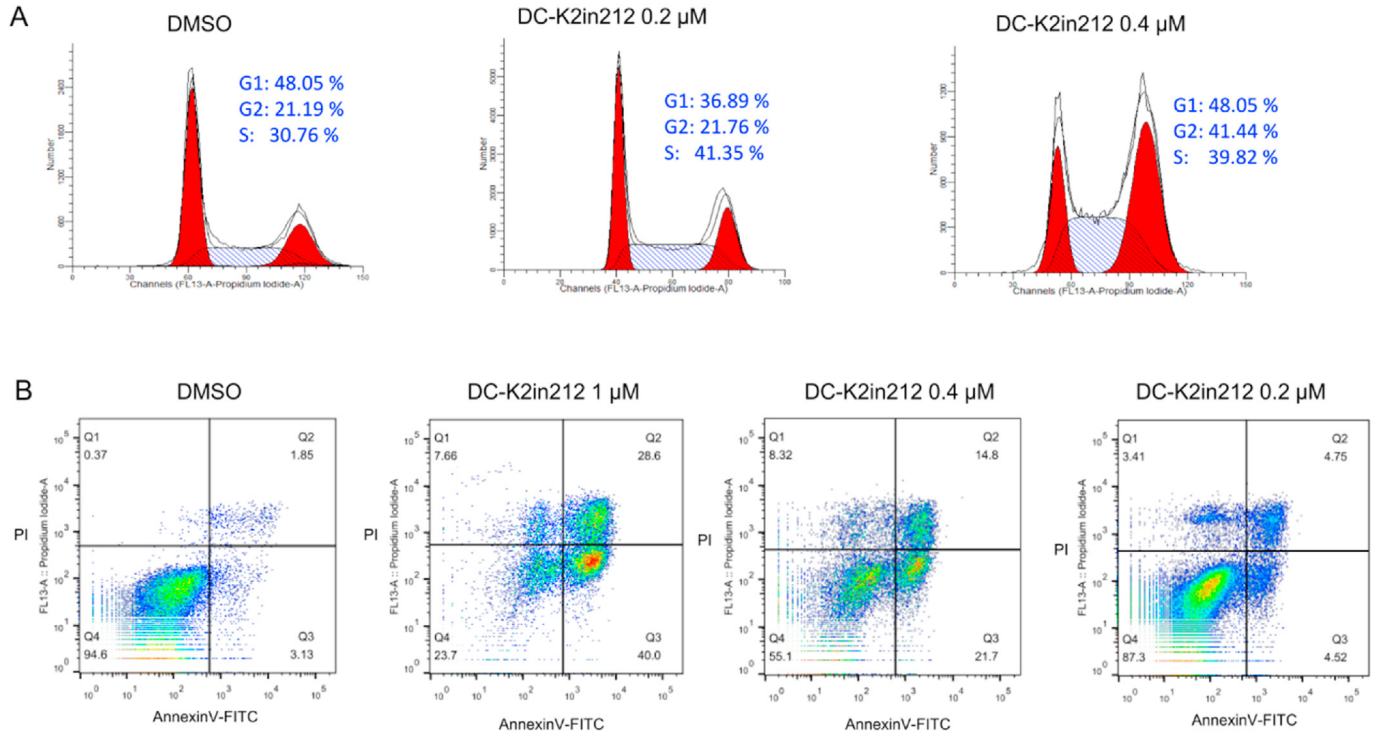

Fig. 5. Effects of **DC-K2in212** on cell cycle and apoptosis of A2058 cells. (A) Cell cycle of A2058 cells treated with **DC-K2in12**. (B) Apoptosis of A2058 cells treated with **DC-K2in212** at different concentrations after 48h.

3. Conclusions

CDK2 has emerged as a promising target for cancer therapy. Due to toxicity caused by poor selectivity of CDK inhibitors, improving selectivity against CDK2 has been an ongoing issue. In this study, we designed, synthesized and evaluated 4-benzoylamino-1H-pyrazole-3-carboxamide derivatives as CDK2 inhibitors. These derivatives showed potent inhibitory activity against CDK2 with IC_{50} values ranging from 6 nM to 485 nM, while having reduced activity against CDK1 with IC_{50} values in the nanomolar to micromolar ranges. Starting from pan-CDK inhibitor AT7519, several compounds were designed and synthesized to validate our design strategy that exploration of the region which is occupied by distal phenyl ring of **C-73** could be a feasible way to improve selectivity of inhibitors against CDK2. Based on this idea further modification was carried out, and finally **DC-K2in212** was discovered as the most selective CDK2 inhibitor in this series. **DC-K2in212** exhibited effective activity against CDK2 with IC_{50} value of 58 nM, meanwhile it had weaker inhibitory activity against other CDK members (CDK1, CDK3, CDK4, CDK6, CDK7, CDK9, and CDK12). Analysis of binding mode illustrated that **DC-K2in212** had the similar binding mode with CDK2 as **C-73**, which might account for its selectivity. Moreover, anti-proliferation assays showed that **DC-K2in212** exhibited impressive activity against A2058 and MV4-11 cancer cell lines and low toxic effect on human normal cell lines MRC5 and LX2. Furthermore, **DC-K2in212** suppressed CDK2-associated downstream signaling pathway, arrested cell cycle, and induced apoptosis. Accordingly, this study discovered a promising CDK2 inhibitor **DC-K2in212** with good selectivity and high potency which could be potential for further development.

4. Experimental

4.1. Chemistry

General methods. All commercial reagents and solvents were obtained from commercial suppliers and used without further purification. Reactions were monitored by thin-layer chromatography (visualized by UV fluorescence at λ = 254 nm). All final compounds were purified by silica gel chromatography with silica gel 60H (200–300 mesh) manufacture by Qingdao Haiyang chemical group Co. (China). ^{1}H, ^{13}C and ^{19}F NMR spectral data were recoded with BURKER AVANCE II 400 M, BURKER AVANCE III 500 M or Varian MR-400 NMR spectrometer. High resolution ESI mass analysis was recorded by Agilent G6520 Q-TOF high resolution mass spectrometer. The purity of all final compounds was determined by Waters UPLC H-Class with ACQUITY UPLC BEH C18 reversed-phase column (2.1 mm × 50 mm, 1.7 μm) and were confirmed to be more than 95%. The analytical method was as follows: flow rate, 0.5 ml/min; eluent A, 0.1% formic acid in water; eluent B, neutral acetonitrile; gradient, 10% B to 100% B in 10min; UV detection at 254 nm.

5. Synthesis and characterization

General procedure A for the synthesis of compounds DC-K2in1, DC-K2in2 and 7 exemplified by compound 7.

N-(4-fluorophenyl)-4-nitro-1H-pyrazole-3-carboxamide (5).A mixture of 4-nitro-1H-pyrazole-3-carboxylic acid (10.000g, 63.69 mmol), 4-fluoroaniline (7.077g, 63.69 mmol), EDCI (12.209g, 63.69 mmol) and HOBt (8.605g, 63.69 mmol) in DMF (200 ml) was stirred at ambient temperature for 2h and poured into water. A precipitate was collected by filtration and concentrated to give the title compound (13.056g, 82%) as brown-white solid. ^{1}H NMR (400 MHz, DMSO-d_6) δ 10.79 (s, 1H), 8.89 (s, 1H), 7.73 (dd, J = 8.9, 5.0 Hz, 2H), 7.21 (t, J = 8.8 Hz, 2H).

4-amino-N-(4-fluorophenyl)-1H-pyrazole-3-carboxamide (6). Compound **6** (5.000g, 20.00 mmol) was dissolved in MeOH (30 ml) and THF (30 ml), catalyzed with 10% Palladium on carbon (500 mg) and then hydrogenated at 40 °C for 36h. The reaction solution was filtrated through Celite and concentrated to give **6** (3.301g, 75%) as a brown foam without further purification.

4-(3-bromo-2,6-difluorobenzamido)-N-(4-fluorophenyl)-1H-pyrazole-3-carboxamide (7). To a solution of compound **6** (3.000g, 13.63 mmol), EDCI (2.613g, 13.63 mmol), and HOBt (1.840g, 13.63 mmol) in DMF (20 ml) was added 3-bromo-2, 6-difluorobenzoic acid (3.230g, 13.63 mmol). The mixture was stirred at ambient temperature for 2h and extracted with ethyl acetate (40 ml × 3). The combined organic layers were dried over anhydrous sodium sulfate and concentrated in vacuum. The residue was purified silica gel chromatography (2% DCM in MeOH) to give compound **7** (4.188g, 70%) as white solid. ^{1}H NMR (400 MHz, DMSO-d_6) δ 13.60 (s, 1H), 10.44 (s, 2H), 8.44 (s, 1H), 7.92 (dd, J = 14.3, 8.3 Hz, 1H), 7.83 (dd, J = 8.5, 5.1 Hz, 2H), 7.28 (t, J = 8.9 Hz, 1H), 7.17 (t, J = 8.7 Hz, 2H).

4-(2,6-difluorobenzamido)-N-(piperidin-4-yl)-1H-pyrazole-3-carboxamide (DC-K2in1). White solid, 69% yield. ^{1}H NMR (400 MHz, MeOD-*d4*) δ 8.35 (s, 1H), 7.62–7.53 (m, 1H), 7.14 (t, J = 8.4 Hz, 2H), 4.20–4.10 (m, 1H), 3.50–3.42 (m, 2H), 3.13 (td, J = 12.6, 2.5 Hz, 2H), 2.17 (dd, J = 13.8, 2.6 Hz, 2H), 1.93–1.82 (m, 2H).

4-(2,6-difluorobenzamido)-N-(4-fluorophenyl)-1H-pyrazole-3-carboxamide (DC-K2in2). White solid, 75% yield. ^{1}H NMR (400 MHz, DMSO-d_6) δ 13.57 (s, 1H), 10.43 (s, 1H), 10.31 (s, 1H), 8.43 (s, 1H), 7.85–7.77 (m, 2H), 7.67–7.57 (m, 1H), 7.26 (t, J = 8.3 Hz, 2H), 7.16 (t, J = 8.9 Hz, 2H).

General procedure B for the synthesis of DC-K2in201 – DC-K2in209, 8 and 9a-9c exemplified by DC-K2in202. To a solution of compound **7** (50 mg, 0.114 mmol), phenylboronic acid (15 mg, 0.125 mmol) and potassium phosphate (36 mg, 0.171 mmol) in the mixture of dioxane (3 ml) and water (1 ml) was added allylpalladium chloride dimer (4 mg, 0.011 mmol) and SSPhos (12 mg, 0.023 mmol) under the protection of argon. The reaction was stirred at 100 °C for 8h. After cooling, the mixture was extracted with ethyl acetate (10 ml × 3) and the combine organic layers were dried over anhydrous sodium sulfate then concentrated in vacuum. The residue was purified by silica gel chromatography (2% DCM in MeOH) to give compound **DC-K2in202** (39 mg, 80%) as white solid. ^{1}H NMR (400 MHz, DMSO-d_6) δ 13.57 (s, 1H), 10.40 (s, 1H), 10.35 (s, 1H), 8.45 (s, 1H), 7.81 (dd, J = 8.7, 5.2 Hz, 2H), 7.71 (dd, J = 15.2, 8.4 Hz, 1H), 7.59–7.43 (m, 5H), 7.35 (t, J = 9.0 Hz, 1H), 7.15 (t, J = 8.9 Hz, 2H). ^{13}C NMR (126 MHz, DMSO-d_6) δ 162.01, 158.58 (dd, $J_{C\text{-}F}$ = 250.9, 6.5 Hz), 158.57 (d, $J_{C\text{-}F}$ = 240.9 Hz),156.81, 156.02 (dd, $J_{C\text{-}F}$ = 252.0, 7.0 Hz), 134.69 (d, $J_{C\text{-}F}$ = 2.0 Hz), 133.93, 133.34, 132.94 (dd, $J_{C\text{-}F}$ = 9.2, 4.3 Hz), 128.90 (d, $J_{C\text{-}F}$ = 1.4 Hz), 128.72, 128.18, 125.51 (dd, $J_{C\text{-}F}$ = 14.2, 3.4 Hz), 122.61 (d, $J_{C\text{-}F}$ = 7.7 Hz), 122.13, 121.61, 115.14 (d, $J_{C\text{-}F}$ = 22.1 Hz), 114.49 (t, $J_{C\text{-}F}$ = 21.5 Hz), 112.49 (dd, $J_{C\text{-}F}$ = 21.6, 2.9 Hz). HRMS $(M + H)^+$ calculated for $C_{23}H_{16}F_3N_4O_2^+$ 437.1220, found 437.1208.

4-(2,6-difluoro-3-(pyridin-3-yl)benzamido)-N-(4-fluorophenyl)-1H-pyrazole-3-carboxamide (DC-K2in201). White solid, 48% yield. ^{1}H NMR (400 MHz, Acetone-*d6*) δ 12.74 (s, 1H), 10.27 (s, 1H), 9.56 (s, 1H), 8.81 (s, 1H), 8.64 (d, J = 4.8 Hz, 1H), 8.54 (s, 1H), 8.01 (d, J = 7.7 Hz, 1H), 7.92–7.85 (m, 2H), 7.79 (dd, J = 15.0, 8.6 Hz, 1H), 7.51 (dd, J = 7.9, 4.8 Hz, 1H), 7.33 (t, J = 8.9 Hz, 1H), 7.13 (t, J = 8.8 Hz, 2H). ^{13}C NMR (126 MHz, DMSO-d_6) δ 161.85, 159.00 (dd, J_{C-F} = 251.4, 6.8 Hz), 158.48 (d, J_{C-F} = 240.7 Hz), 156.57, 156.19 (dd, J_{C-F} = 252.3, 7.1 Hz), 149.24 (d, J_{C-F} = 2.7 Hz), 149.17, 136.41, 134.63 (d, J_{C-F} = 2.0 Hz), 133.37, 133.04 (dd, J_{C-F} = 9.5, 4.1 Hz), 129.85, 123.73, 122.57 (d, J_{C-F} = 7.7 Hz), 122.28 (dd, J_{C-F} = 14.4,

3.3 Hz), 121.88, 121.67, 115.13 (d, J_{C-F} = 22.2 Hz), 114.60 (t, J_{C-F} = 21.6 Hz), 112.78 (dd, J_{C-F} = 21.8, 2.9 Hz). HRMS (M + H)$^+$ calculated for $C_{22}H_{15}F_3N_5O_2^+$ 438.1172, found 438.1173.

4-(2,6-difluoro-3-(6-fluoropyridin-3-yl)benzamido)-N-(4-fluorophenyl)-1H-pyrazole-3-carboxamide(DC-K2in203). White solid, 38% yield. ^{1}H NMR (400 MHz, Acetone-*d6*) δ 12.70 (s, 1H), 10.25 (s, 1H), 9.55 (s, 1H), 8.54 (s, 1H), 8.46 (s, 1H), 8.25–8.17 (m, 1H), 7.90 (dd, *J* = 9.1, 4.9 Hz, 2H), 7.80 (td, *J* = 8.7, 6.2 Hz, 1H), 7.34 (td, *J* = 8.9, 1.3 Hz, 1H), 7.25 (dd, *J* = 8.6, 2.9 Hz, 1H), 7.13 (t, *J* = 8.9 Hz, 2H). ^{13}C NMR (126 MHz, DMSO-d_6) δ 162.75 (d, J_{C-F} = 237.6 Hz), 161.90, 159.09 (dd, J_{C-F} = 251.7, 6.7 Hz), 158.53 (d, J_{C-F} = 240.8 Hz), 156.51, 156.18 (dd, J_{C-F} = 252.4, 7.0 Hz), 147.33 (d, J_{C-F} = 15.3 Hz), 142.44 (d, J_{C-F} = 6.4 Hz), 134.63 (d, J_{C-F} = 1.7 Hz), 133.33, 133.02 (d, J_{C-F} = 5.8 Hz), 128.20 (d, J_{C-F} = 3.6 Hz), 122.58 (d, J_{C-F} = 7.6 Hz), 121.95, 121.64, 121.18 (dd, J_{C-F} = 14.0, 2.3 Hz), 115.12 (d, J_{C-F} = 22.2 Hz), 114.57 (t, J_{C-F} = 21.5 Hz), 112.75 (dd, J_{C-F} = 21.9, 2.4 Hz), 109.64 (d, J_{C-F} = 37.8 Hz). HRMS (M + H)$^+$ calculated for $C_{22}H_{14}F_4N_5O_2^+$ 456.1078, found 456.1079.

4-(2,6-difluoro-3-(6-methylpyridin-3-yl)benzamido)-N-(4-fluorophenyl)-1H-pyrazole-3-carboxamide (DC-K2in204). White solid, 49% yield. ^{1}H NMR (400 MHz, Acetone-*d6*) δ 12.70 (s, 1H), 10.25 (s, 1H), 9.54 (s, 1H), 8.73 (s, 1H), 8.53 (s, 1H), 7.94–7.84 (m, 3H), 7.76 (dd, *J* = 15.0, 8.5 Hz, 1H), 7.39 (d, *J* = 8.0 Hz, 1H), 7.32 (t, *J* = 8.8 Hz, 1H), 7.12 (t, *J* = 8.8 Hz, 2H), 2.59 (s, 3H). ^{13}C NMR (126 MHz, DMSO-d_6) δ 161.94, 158.86 (dd, J_{C-F} = 251.6, 6.7 Hz), 158.54 (d, J_{C-F} = 240.9 Hz), 157.78, 156.64, 156.22 (dd, J_{C-F} = 252.2, 6.9 Hz), 148.45 (d, J_{C-F} = 2.1 Hz), 136.50, 134.67, 133.36, 132.83 (d, J_{C-F} = 5.1 Hz), 126.92, 123.01, 122.59 (d, J_{C-F} = 7.6 Hz), 122.43 (d, J_{C-F} = 14.9 Hz), 122.03, 121.65, 115.13 (d, J_{C-F} = 22.2 Hz), 114.56 (t, J_{C-F} = 21.4 Hz), 112.70 (d, J_{C-F} = 20.1 Hz), 23.74. HRMS (M + H)$^+$ calculated for $C_{23}H_{17}F_3N_5O_2^+$ 452.1329, found 452.1339.

4-(2,6-difluoro-3-(6-methoxypyridin-3-yl)benzamido)-N-(4-fluorophenyl)-1H-pyrazole-3-carboxamide(DC-K2in205). White solid, 51% yield. ^{1}H NMR (400 MHz, Acetone-*d6*) δ 12.68 (s, 1H), 10.25 (s, 1H), 9.56 (s, 1H), 8.54 (s, *J* = 9.6 Hz, 1H), 8.38 (s, 1H), 7.94–7.87 (m, 3H), 7.73 (dd, *J* = 15.1, 8.7 Hz, 1H), 7.29 (t, *J* = 8.7 Hz, 1H), 7.12 (t, *J* = 8.8 Hz, 2H), 6.90 (d, *J* = 8.6 Hz, 1H), 3.94 (s, 3H). ^{13}C NMR (126 MHz, DMSO-d_6) δ 163.36, 161.93, 158.59 (dd, J_{C-F} = 251.8, 7.6 Hz), 158.51 (d, J_{C-F} = 240.6 Hz), 156.64, 156.08 (dd, J_{C-F} = 251.8, 7.0 Hz), 146.62(d, J_{C-F} = 2.4 Hz), 139.44, 134.64 (d, J_{C-F} = 1.8 Hz), 133.30, 132.65 (d, J_{C-F} = 9.0 Hz), 123.19, 122.57 (d, J_{C-F} = 7.7 Hz), 122.27 (dd, J_{C-F} = 14.3, 3.0 Hz), 122.00, 121.58, 115.12 (d, J_{C-F} = 22.1 Hz), 114.47 (t, J_{C-F} = 21.4 Hz), 112.60 (dd, J_{C-F} = 21.8, 2.6 Hz), 110.52, 53.34. HRMS (M + H)$^+$ calculated for $C_{23}H_{17}F_3N_5O_3^+$ 468.1278, found 468.1273.

4-(3-(6-aminopyridin-3-yl)-2,6-difluorobenzamido)-N-(4-fluorophenyl)-1H-pyrazole-3-carboxamide(DC-K2in206). White solid, 36% yield. ^{1}H NMR (400 MHz, MeOD-*d4*) δ 8.41 (s, 1H), 8.11 (s, 1H), 7.75–7.67 (m, 3H), 7.62 (dd, *J* = 15.0, 8.7 Hz, 1H), 7.19 (t, *J* = 8.9 Hz, 1H), 7.07 (t, *J* = 8.8 Hz, 2H), 6.70 (d, *J* = 8.7 Hz, 1H). ^{13}C NMR (126 MHz, DMSO-d_6) δ 161.92, 158.53 (d, J_{C-F} = 240.9 Hz), 157.86 (dd, J_{C-F} = 256.2, 6.6 Hz), 156.92, 159.53, 155.85 (dd, J_{C-F} = 250.6, 6.8 Hz), 147.70(d, J_{C-F} = 3.1 Hz), 137.41, 134.63 (d, J_{C-F} = 2.2 Hz), 133.31, 131.96 (dd, J_{C-F} = 8.9, 4.8 Hz), 123.41 (dd, J_{C-F} = 14.4, 3.3 Hz), 122.63 (d, J_{C-F} = 7.8 Hz), 122.01, 121.63, 117.74, 115.17 (d, J_{C-F} = 22.2 Hz), 114.43 (t, J_{C-F} = 21.6 Hz), 112.46 (dd, J_{C-F} = 21.6, 2.7 Hz), 107.83. HRMS (M + H)$^+$ calculated for $C_{22}H_{16}F_3N_6O_2^+$ 453.1281, found 453.1274.

4-(2,4-difluoro-3′-hydroxy-[1,1′-biphenyl]-3-carboxamido)-N-(4-fluorophenyl)-1H-pyrazole-3-carboxamide(DC-K2in207). White solid, 54%. ^{1}H NMR (400 MHz, DMSO-d_6) δ 13.58 (s, 1H), 10.42 (s, 1H), 10.36 (s, 1H), 9.65 (s, 1H), 8.45 (s, 1H), 7.84–7.77 (m, 2H), 7.66 (td, *J* = 8.8, 6.5 Hz, 1H), 7.35–7.28 (m, 2H), 7.19–7.12 (m, 2H), 6.97–6.93 (m, 2H), 6.85–6.82 (m, 1H). ^{13}C NMR (126 MHz, DMSO-d_6) δ 161.87, 158.41 (dd, J_{C-F} = 251.3, 7.3 Hz), 157.67 (d, J_{C-F} = 215.7 Hz), 157.56, 156.94–154.77 (m), 135.09, 134.64 (d, J_{C-F} = 2.1 Hz), 133.36, 132.84 (dd, J_{C-F} = 9.0, 4.1 Hz), 129.82, 125.56 (dd, J_{C-F} = 14.4, 3.2 Hz), 122.59 (d, J_{C-F} = 7.8 Hz), 121.91, 121.61, 119.59, 115.80, 115.28, 115.15 (d, J_{C-F} = 22.2 Hz), 114.48 (t, J_{C-F} = 21.8 Hz), 112.46 (dd, J_{C-F} = 22.0, 2.8 Hz). HRMS (M + H)$^+$ calculated for $C_{23}H_{16}F_3N_4O_3^+$ 453.1169, found 453.1164.

4-(2,4-difluoro-3′-(hydroxymethyl)-[1,1′-biphenyl]-3-carboxamido)-N-(4-fluorophenyl)-1H-pyrazole-3-carboxamide(DC-K2in208). White solid, 58%. ^{1}H NMR (400 MHz, DMSO-d_6) δ 13.58 (s, 1H), 10.43 (s, 1H), 10.37 (s, 1H), 8.45 (s, 1H), 7.81 (dd, *J* = 9.1, 5.1 Hz, 2H), 7.70 (td, *J* = 8.7, 6.4 Hz, 1H), 7.50 (s, 1H), 7.48–7.32 (m, 4H), 7.15 (t, *J* = 8.9 Hz, 2H), 5.28 (t, *J* = 5.7 Hz, 1H), 4.57 (d, *J* = 5.7 Hz, 2H). ^{13}C NMR (126 MHz, DMSO-d_6) δ 162.02, 158.60 (d, J_{C-F} = 240.8 Hz), 159.66–157.51 (m), 156.90, 156.06 (dd, J_{C-F} = 251.8, 6.9 Hz), 143.25, 134.71 (d, J_{C-F} = 1.7 Hz), 133.81, 133.41, 132.99 (dd, J_{C-F} = 8.5, 3.5 Hz), 128.60, 127.32, 127.06, 126.44, 125.73 (dd, J_{C-F} = 14.3, 3.2 Hz), 122.68 (d, J_{C-F} = 7.7 Hz), 122.11, 121.69, 115.22 (d, J_{C-F} = 22.1 Hz), 114.53 (t, J_{C-F} = 21.5 Hz), 112.56 (dd, J_{C-F} = 21.5, 2.1 Hz), 62.93. HRMS (M + H)$^+$ calculated for $C_{24}H_{18}F_3N_4O_3^+$ 467.1326, found 467.1333.

2,4-difluoro-N3-(3-((4-fluorophenyl)carbamoyl)-1H-pyrazol-4-yl)-[1,1′-biphenyl]-3,3′-dicarboxamide(DC-K2in209). White solid, 60%. ^{1}H NMR (400 MHz, DMSO-d_6) δ 13.60 (s, 1H), 10.44 (s, 1H), 10.39 (s, 1H), 8.46 (s, 1H), 8.10 (s, 1H), 8.06 (s, 1H), 7.94 (d, *J* = 7.7 Hz, 1H), 7.87–7.74 (m, 3H), 7.72 (d, *J* = 7.7 Hz, 1H), 7.59 (t, *J* = 7.7 Hz, 1H), 7.48 (s, 1H), 7.39 (t, *J* = 8.7 Hz, 1H), 7.15 (t, *J* = 8.8 Hz, 2H). ^{13}C NMR (126 MHz, DMSO-d_6) δ 167.69, 161.92, 158.70 (dd, J_{C-F} = 250.9, 6.6 Hz), 158.53 (d, J_{C-F} = 240.1 Hz), 156.76, 156.03 (dd, J_{C-F} = 251.0, 5.8 Hz), 134.89, 134.63, 133.94, 133.39, 133.13 (d, J_{C-F} = 8.2 Hz), 131.71, 128.79, 128.10, 127.39, 124.95 (dd, J_{C-F} = 14.0, 3.2 Hz), 121.93, 121.95 (d, J_{C-F} = 6.1 Hz), 121.68, 115.17 (d, J_{C-F} = 22.2 Hz), 114.55 (t, J_{C-F} = 21.8 Hz), 112.64 (d, J_{C-F} = 21.5 Hz). HRMS (M + H)$^+$ calculated for $C_{24}H_{17}F_3N_5O_3^+$ 480.1278, found 480.1289.

4-(3-(6-cyanopyridin-3-yl)-2,6-difluorobenzamido)-N-(4-fluorophenyl)-1H-pyrazole-3-carboxamide(8). White solid, 49% yield. ^{1}H NMR (400 MHz, DMSO-d_6) δ 13.58 (s, 1H), 10.39 (d, *J* = 3.9 Hz, 2H), 8.97 (s, 1H), 8.45 (s, 1H), 8.29 (d, *J* = 8.1 Hz, 1H), 8.19 (d, *J* = 8.2 Hz, 1H), 7.90 (dd, *J* = 15.0, 8.5 Hz, 1H), 7.81 (dd, *J* = 8.4, 5.1 Hz, 2H), 7.46 (t, *J* = 9.0 Hz, 1H), 7.15 (t, *J* = 8.7 Hz, 2H).

Methyl 2′,4′-difluoro-3′-((3-((4-fluorophenyl)carbamoyl)-1H-pyrazol-4-yl)carbamoyl)-[1,1′-biphenyl]-3-carboxylate(DC-K2in211(9a)). White solid, 81%. ^{1}H NMR (400 MHz, DMSO-d_6) δ 13.60 (s, 1H), 10.45 (s, 1H), 10.40 (s, 1H), 8.46 (s, 1H), 8.12 (d, *J* = 1.4 Hz, 1H), 8.03 (dd, *J* = 6.5, 1.4 Hz, 1H), 7.89–7.74 (m, 4H), 7.68 (t, *J* = 7.8 Hz, 1H), 7.38 (t, *J* = 8.7 Hz, 1H), 7.20–7.11 (m, 2H), 3.88 (s, 3H). ^{13}C NMR (126 MHz, DMSO-d_6) δ 165.94, 161.94, 158.87 (dd, J_{C-F} = 251.2, 6.4 Hz), 158.53 (d, J_{C-F} = 241.0 Hz), 156.67, 156.12 (dd, J_{C-F} = 252.5, 6.7 Hz), 134.70, 134.32, 133.51, 133.36, 132.97 (d, J_{C-F} = 5.8 Hz), 130.18, 129.52, 129.24, 128.88, 124.38 (d, J_{C-F} = 13.8 Hz), 122.55 (d, J_{C-F} = 7.3 Hz), 122.05, 121.65, 115.13 (d, J_{C-F} = 22.1 Hz), 114.56 (t, J_{C-F} = 21.5 Hz), 112.66 (d, J_{C-F} = 21.2 Hz), 52.24. HRMS (M + H)$^+$ calculated for $C_{25}H_{18}F_3N_4O_4^+$ 495.1275, found 495.1277.

Methyl 2′, 4′, 6-trifluoro-3′-((3-((4-fluorophenyl) carbamoyl)-1H-pyrazol-4-yl)carbamoyl)-[1,1′-biphenyl]-3-carboxylate (9b) White solid, 68% yield. ^{1}H NMR (400 MHz, MeOD-*d4*) δ 8.39 (s, 1H), 8.11–8.05 (m, 2H), 7.69–7.64 (m, 2H), 7.60 (dd, *J* = 14.7, 8.4 Hz, 1H), 7.30 (t, *J* = 9.4 Hz, 1H), 7.22 (t, *J* = 8.5 Hz, 1H), 7.03 (t, *J* = 8.8 Hz, 2H), 3.88 (s, 3H).

Methyl 2′, 4′-difluoro-3′-((3-((4-fluorophenyl)carbamoyl)-1H-pyrazol-4-yl)carbamoyl)-6-methyl-[1,1′-biphenyl]-3-carboxylate (9c) White solid, 72% yield. ^{1}H NMR (400 MHz, MeOD-*d4*) δ 8.38 (s, 1H), 7.91 (dd, *J* = 8.0, 1.7 Hz, 1H), 7.82 (d, *J* = 1.6 Hz, 1H), 7.68–7.63

(m, 2H), 7.43 (td, J = 8.4, 6.4 Hz, 1H), 7.37 (d, J = 8.1 Hz, 1H), 7.18 (t, J = 8.8 Hz, 1H), 7.05–6.98 (m, 2H), 3.85 (s, 3H), 2.23 (d, J = 7.4 Hz, 3H).

5-(2,4-difluoro-3-((3-((4-fluorophenyl)carbamoyl)-1H-pyrazol-4-yl)carbamoyl)phenyl) picolinamide (DC-K2in212). To a suspension of compound **8** (50 mg, 0.108 mmol) in the mixture of H_2O (3 ml) and MeOH (3 ml), and NaOH (18 mg, 0.432 mmol) was added and stirred at 60 °C for 2h. After cooling, the mixture was treated with 2 M HCl to neutral and extracted with ethyl acetate (5 ml × 3).The combine organic layers were dried over anhydrous sodium sulfate then concentrated in vacuum. The residue was purified by silica gel chromatography (5% DCM:MeOH) to give compound **DC-K2in212** (18 mg, 35%) as white solid. ^{1}H NMR (400 MHz, DMSO-d_6) δ 13.60 (s, 1H), 10.42 (s, 1H), 10.40 (s, 1H), 8.82 (s, 1H), 8.45 (s, 1H), 8.24–8.13 (m, 3H), 7.88 (td, J = 8.7, 6.5 Hz, 1H), 7.81 (dd, J = 9.1, 5.1 Hz, 2H), 7.72 (s, 1H), 7.44 (t, J = 8.7 Hz, 1H), 7.15 (t, J = 8.9 Hz, 2H). ^{13}C NMR (126 MHz, DMSO-d_6) δ 165.75, 161.81, 159.27 (dd, J_{C-F} = 252.2, 6.6 Hz), 158.47 (d, J_{C-F} = 240.7 Hz), 156.49, 156.27 (dd, J_{C-F} = 252.7, 7.1 Hz), 149.74, 148.15, 137.82, 134.61 (d, J_{C-F} = 1.7 Hz), 133.39, 133.18 (d, J_{C-F} = 7.6 Hz), 132.21, 122.57 (d, J_{C-F} = 7.7 Hz), 121.96, 121.80, 121.74–121.51 (m), 115.14 (d, J_{C-F} = 22.1 Hz), 114.69 (t, J_{C-F} = 21.7 Hz), 112.92 (d, J_{C-F} = 19.4 Hz).HRMS (M + H)$^+$ calculated for $C_{23}H_{16}F_3N_6O_3^+$ 481.1230, found 481.1239.

General procedure C for the synthesis of compounds *10a-10c*. To a suspension of compounds **9a-9c** (1.0 eq) in the mixture of H_2O (5 ml) and MeOH (5 ml), and LiOH·H_2O (4.0 eq) was added and stirred at 40 °C for 4h. After cooling, the mixture was treated with 2 M HCl. An amount of white solid was precipitated, filtered off, washed with water and dried to afford compounds **10a-10c** without further purification.

2′,4′-difluoro-3'-((3-((4-fluorophenyl)carbamoyl)-1H-pyrazol-4-yl)carbamoyl)-[1,1′-biphenyl]-3-carboxylic acid (10a) White solid, 89% yield. ^{1}H NMR (400 MHz, DMSO) δ 13.60 (s, 1H), 13.18 (s, 1H), 10.43 (s, 1H), 10.40 (s, 1H), 8.45 (s, 1H), 8.10 (s, 1H), 8.01 (d, J = 7.8 Hz, 1H), 7.85–7.74 (m, 4H), 7.65 (t, J = 7.8 Hz, 1H), 7.38 (t, J = 8.6 Hz, 1H), 7.15 (t, J = 8.9 Hz, 2H).

2′,4′,6-trifluoro-3'-((3-((4-fluorophenyl)carbamoyl)-1H-pyrazol-4-yl)carbamoyl)-[1,1′-biphenyl]-3-carboxylic acid (10b) White solid, 85% yield. ^{1}H NMR (400 MHz, DMSO) δ 13.63 (s, 1H), 13.25 (s, 1H), 10.44 (s, 1H), 10.41 (s, 1H), 8.44 (s, 1H), 8.12–8.02 (m, 2H), 7.82 (dd, J = 8.9, 5.0 Hz, 2H), 7.76 (dd, J = 15.1, 8.6 Hz, 1H), 7.51 (t, J = 9.2 Hz, 1H), 7.41 (t, J = 8.8 Hz, 1H), 7.16 (t, J = 8.9 Hz, 2H).

2′,4′-difluoro-3'-((3-((4-fluorophenyl)carbamoyl)-1H-pyrazol-4-yl)carbamoyl)-6-methyl-[1,1′-biphenyl]-3-carboxylic acid (10c) White solid, 93% yield. ^{1}H NMR (400 MHz, DMSO) δ 13.61 (s, 1H), 13.03 (s, 1H), 10.44 (s, 1H), 10.40 (s, 1H), 8.44 (s, 1H), 7.91 (dd, J = 7.9, 1.5 Hz, 1H), 7.85–7.77 (m, 3H), 7.59 (dd, J = 15.0, 8.5 Hz, 1H), 7.49 (d, J = 8.0 Hz, 1H), 7.36 (t, J = 8.8 Hz, 1H), 7.16 (t, J = 8.9 Hz, 2H), 2.24 (s, 3H).

General procedure D for the synthesis of compounds *DC-K2in213 – DC-K2in217 exemplified by DC-K2in213.*

A mixture of compound **10a** (50 mg, 0.104 mmol), (1-Methyl-4-piperidyl)methanamine (13 mg, 0.104 mmol), EDCI (20 mg, 0.104 mmol) and HOBt (14 mg, 0.104 mmol) in DMF (0.6 ml) was stirred at ambient temperature for 18h. Water (1.2 ml) was added to the mixture, and extracted with ether acetate (6ml × 6).The combined organic layers were dried over anhydrous sodium sulfate then concentrated in vacuum. The residue was purified by silica gel chromatography (10% MeOH in DCM) to afford compound **DC-K2in213** (21 mg, 35%). ^{1}H NMR (400 MHz, DMSO-d_6) δ 13.68 (s, 1H), 10.45 (s, 1H), 10.38 (s, 1H), 8.73 (t, J = 5.7 Hz, 1H), 8.43 (s, 1H), 8.03 (s, 1H), 7.92 (d, J = 7.8 Hz, 1H), 7.85–7.76 (m, 3H), 7.72 (d, J = 7.3 Hz, 1H), 7.60 (t, J = 7.8 Hz, 1H), 7.39 (t, J = 8.8 Hz, 1H), 7.15 (t, J = 8.9 Hz, 2H), 3.34–3.27 (m, 2H), 3.26–3.18 (m, 2H), 2.82 (t, J = 11.6 Hz, 2H), 2.65 (s, 3H), 1.89–1.74 (m, 3H), 1.53–1.39 (m, 2H). ^{13}C NMR (126 MHz, DMSO-d_6) δ 166.31, 162.17, 159.04 (dd, J_{C-F} = 250.8, 6.7 Hz), 158.87 (d, J_{C-F} = 240.6 Hz), 157.11, 156.34 (dd, J_{C-F} = 252.0, 7.3 Hz), 135.60, 135.04 (d, J_{C-F} = 2.0 Hz), 134.32, 133.60(m), 131.93,130.10, 129.21, 128.06, 127.55, 125.34 (dd, J_{C-F} = 14.0, 3.2 Hz), 122.98 (d, J_{C-F} = 7.8 Hz), 122.25, 115.57 (d, J_{C-F} = 22.2 Hz), 114.94 (t, J_{C-F} = 21.7 Hz), 113.07 (dd, J_{C-F} = 21.5, 2.8 Hz), 55.32, 46.19, 45.20, 35.33, 29.93. HRMS (M + H)$^+$ calculated for $C_{31}H_{30}F_3N_6O_3^+$ 591.2326, found 591.2315.

2,4-difluoro-N3-(3-((4-fluorophenyl)carbamoyl)-1H-pyrazol-4-yl)-N3'-(2-(4-methylpiperazin-1-yl)ethyl)-[1,1′-biphenyl]-3,3′-dicarboxamide (DC-K2in214). White solid, 30% yield. ^{1}H NMR (400 MHz, DMSO-d_6) δ 13.61 (s, 1H), 10.43 (s, 1H), 10.39 (s, 1H), 8.52 (t, J = 5.6 Hz, 1H), 8.46 (s, 1H), 8.01 (s, 1H), 7.89 (d, J = 7.8 Hz, 1H), 7.85–7.74 (m, 3H), 7.71 (d, J = 7.0 Hz, 1H), 7.59 (t, J = 7.7 Hz, 1H), 7.38 (t, J = 8.7 Hz, 1H), 7.19–7.10 (m, 2H), 3.40–3.35 (m, 2H), 2.48–2.24 (m, 10H), 2.11 (s, 3H). ^{13}C NMR (126 MHz, DMSO-d_6) δ 165.77, 161.76, 158.62 (dd, J_{C-F} = 250.4, 6.3 Hz), 158.44 (d, J_{C-F} = 240.7 Hz), 156.65, 155.92 (dd, J_{C-F} = 252.1, 7.3 Hz), 135.14, 134.59 (d, J_{C-F} = 2.0 Hz), 133.88, 133.17, 133.08 (d, J_{C-F} = 6.1 Hz), 131.48, 128.82, 127.63, 127.03, 124.86 (dd, J_{C-F} = 14.1, 3.1 Hz), 122.55 (d, J_{C-F} = 7.8 Hz), 121.85, 121.80, 115.12 (d, J_{C-F} = 22.2 Hz), 114.43 (d, J_{C-F} = 21.5 Hz), 112.63 (dd, J_{C-F} = 21.8, 2.6 Hz), 56.90, 54.73, 52.67, 45.69, 36.97. HRMS (M + H)$^+$ calculated for $C_{31}H_{31}F_3N_7O_3^+$ 606.2435, found 606.2450.

2,4-difluoro-N3-(3-((4-fluorophenyl)carbamoyl)-1H-pyrazol-4-yl)-N3'-(3-morpholinopropyl)-[1,1′-biphenyl]-3,3′-dicarboxamide (DC-K2in215). White solid, 32% yield.^{1}H NMR (400 MHz, DMSO-d_6) δ 13.61 (s, 1H), 10.45 (s, 1H), 10.39 (s, 1H), 8.61 (t, J = 5.5 Hz, 1H), 8.45 (s, 1H), 8.01 (s, 1H), 7.90 (d, J = 7.8 Hz, 1H), 7.84–7.75 (m, 3H), 7.71 (d, J = 7.7 Hz, 1H), 7.59 (t, J = 7.7 Hz, 1H), 7.40 (t, J = 8.5 Hz, 1H), 7.19–7.12 (m, 2H), 3.55 (t, J = 4.5 Hz, 4H), 3.31 (dd, J = 12.8, 6.8 Hz, 2H), 2.38–2.29 (m, 6H), 1.74–1.65 (m, 2H)· ^{13}C NMR (126 MHz, DMSO-d_6) δ 165.80, 161.82, 158.67 (dd, J_{C-F} = 251.2, 6.8 Hz), 158.49 (d, J_{C-F} = 240.7 Hz), 156.68, 155.98 (dd, J_{C-F} = 252.2, 6.9 Hz), 135.22, 134.63 (d, J_{C-F} = 2.2 Hz), 133.92, 133.12 (dd, J_{C-F} = 9.6, 4.3 Hz), 131.48, 128.79, 127.65, 127.05, 124.93 (dd, J_{C-F} = 14.2, 3.3 Hz), 122.58 (d, J_{C-F} = 7.8 Hz), 121.92, 121.77, 115.14 (d, J_{C-F} = 22.2 Hz), 114.51 (t, J_{C-F} = 21.6 Hz), 112.64 (dd, J_{C-F} = 21.7, 2.5 Hz), 66.25, 56.17, 53.38, 37.91, 26.00. HRMS (M + H)$^+$ calculated for $C_{31}H_{30}F_3N_6O_4^+$ 607.2202, found 607.2253.

2,4,6′-trifluoro-N3-(3-((4-fluorophenyl)carbamoyl)-1H-pyrazol-4-yl)-N3'-(3-morpholinopropyl)-[1,1′-biphenyl]-3,3′-dicarboxamide (DC-K2in216). White solid, 26% yield. ^{1}H NMR (400 MHz, MeOD-*d4*) δ 8.41 (s, 1H), 7.99–7.93 (m, 2H), 7.72–7.63 (m, 3H), 7.35 (t, J = 9.1 Hz, 1H), 7.28 (t, J = 9.0 Hz, 1H), 7.07 (dd, J = 12.1, 5.5 Hz, 2H), 3.69 (t, J = 4.6 Hz, 4H), 3.44 (t, J = 6.9 Hz, 2H), 2.57–2.46 (m, 6H), 1.90–1.79 (m, 2H). HRMS (M + H)$^+$ calculated for $C_{31}H_{29}F_4N_6O_4^+$ 625.2181, found 625.2183.

2,4-difluoro-N3-(3-((4-fluorophenyl)carbamoyl)-1H-pyrazol-4-yl)-6′-methyl-N3'-(3-morpholinopropyl)-[1,1′-biphenyl]-3,3′-dicarboxamide (DC-K2in217). White solid, 28% yield.^{1}H NMR (400 MHz, MeOD-*d4*) δ 8.40 (s, 1H), 7.80 (dd, J = 8.0, 1.9 Hz, 1H), 7.71–7.66 (m, 3H), 7.50 (dd, J = 14.8, 8.3 Hz, 1H), 7.43 (d, J = 8.0 Hz, 1H), 7.24 (t, J = 8.8 Hz, 1H), 7.10–7.03 (m, 2H), 3.66 (t, J = 4.6 Hz, 4H), 3.42 (t, J = 6.8 Hz, 2H), 2.56–2.46 (m, 6H), 2.26 (s, 3H), 1.88–1.77 (m, 2H). ^{13}C NMR (126 MHz, DMSO-d_6) δ 166.15, 161.95, 158.88 (dd, J_{C-F} = 250.8, 6.5 Hz), 158.59 (d, J_{C-F} = 240.8 Hz), 156.64, 155.96 (dd, J_{C-F} = 250.0, 7.0 Hz), 139.92, 134.64 (d, J_{C-F} = 1.7 Hz), 133.98–133.69 (m), 133.12, 132.16, 130.21, 129.03, 127.52, 124.98 (dd, J_{C-F} = 17.4, 3.0 Hz), 122.66 (d, J_{C-F} = 7.7 Hz), 122.04, 121.79, 115.15 (d, J_{C-F} = 22.2 Hz), 114.10 (t, J_{C-F} = 21.2 Hz), 112.42 (d, J_{C-F} = 19.7 Hz), 63.48, 54.29, 51.23, 36.51, 23.75, 19.48. HRMS (M + H)$^+$ calculated for $C_{32}H_{32}F_3N_6O_4^+$ 621.2432, found 621.2432.

5.1. Biology methods

5.1.1. Kinase assays

The kinase inhibition was detected by mobility shift assay. Briefly, active kinases, FAM-labeled peptides and ATP were diluted with kinase base buffer (50 mM HEPES, pH 7.5, 0.0015% Brij-35), respectively. Then 10 μl of kinase solution was added to each well of the 384-well assay plate, which already contains 5 μl of serially diluted compound in 10% DMSO in each well, and incubated at room temperature for 10 min. Then 5 μl of peptide solution and 5 μl of ATP solution were added to each well of the 384-well assay plate. After incubation at 28 °C for specified time, kinase reactions were stopped by 25 μl of stop buffer (100 mM HEPES, pH 7.5, 0.015% Brij-35, 0.2% Coating Reagent #3 and 50 mM EDTA). Data were collected on Caliper (PerkinElmer, Caliper EZ ReaderII). The source of the active CDKs/cyclins proteins and FAM-labeled peptides were shown in Table S1.

5.1.2. Cell culture and viability assay

A2058, LX2 and MRC5 cells were cultured in Dulbecco's Modified Eagle's Medium (DMEM, Invitrogen), while MV4-11 cells were cultured in RPMI 1640 medium Medium (Invitrogen). Both medium were supplemented with 10% fetal bovine, 1% penicillin and streptomycin (Invitrogen). For cell viability assay, cells were plated in 96-well plates in a volume of 100 μl and treated with compounds in corresponding concentration (DMSO as control) for 96 h. Cell viability was determined by CellTiter-Glo® Luminescent Cell Viability assay kit (Promega).

5.1.3. Western blot

Total cell lysates were separated by 8% or 10% SDS-polyacrylamide gels and transferred to nitrocellulose membranes. The blots were blocked with blocking buffer (5% non-fat milk in TBST) for 60 min at room temperature and incubated with primary antibodies overnight at 4 °C. Then the blots were washed three times with TBST and incubated with 1:10,000 dilution of secondary antibody (HRP conjugated) for 1 h. Following another three washes, bands were detected in a ChemiScope3400 imaging system using ECL substrate (Clinx). Primary antibodies used were as follows: anti-Mcl-1 (Cell Signaling Technology, no.5453T), anti-Rb (Cell Signaling Technology, no.9309T), anti-Phospho-Rb (Ser780) (Cell Signaling Technology, no.8180T), anti-Phospho-Rb (Ser807/811) (Cell Signaling Technology, no.8516T), anti-Cleaved Caspase-3 (Cell Signaling Technology, no.9661S), anti-Cleaved PARP (Cell Signaling Technology, no.5625T), anti- GAPDH (Cell Signaling Technology, no.5174S), and anti-Tubulin (Cell Signaling Technology, no.9873S).

5.1.4. Flow cytometric analysis

A2058 cells were plated in 6-cm dishes, and after 24 h, cells were treated with compounds or DMSO control. For cell cycle analysis, cells were harvested at 24 h and gently resuspended in 70% ethanol overnight at 4 °C for fixation. Then samples were washed with PBS twice and incubated with Propidium Iodide/RNase Staining Buffer (BD Pharmingen) for 20 min at room temperature. For cell apoptosis analysis, cells were harvested at 48 h and were measured using Annexin V-FITC Apoptosis Detection Kit (Vazyme Biotech) according to the manufacturer's instructions. Samples were detected by BD FACSCalibur (BD Pharmingen), and data were analyzed by FlowJo V7.6.1.

5.1.5. SiRNA transfection

SiRNA duplex oligonucleotides against human CDK2 and a non-targeting negative control siRNA were synthesized by Genepharma. A2058 cells were seeded in six-well plates (Corning) at a density of 5×10^5 cells per well and allowed to adhere overnight. The cell culture medium was changed to Opti-MEM medium (Invitrogen, Cat #11058021) before transfection. SiRNA-Lipofectamine mixture was prepared using Lipofectamine RNAiMAX Transfection Reagent (Invitrogen, Cat# 13,778,100) as manufacturer's instructions. After 6 h, Opti-MEM medium was switched to culture medium and incubated for 48 h. Western blot assays were used to detect the expression of CDK2 protein. The sequence of the SiRNA duplex oligonucleotides were as followed. Si-CDK2-1#: (Sense, 5′-3′) CCAGCUCUUCCGGAUCUUUTT, (Antisense, 5′-3′) AAAGAUCCGGAAGAGCUGGTT.

Si-CDK2-2#: (Sense, 5′-3′) CCAGCUCUUCCGGAUCUUUTT, (Antisense, 5′-3′)AAAGAUCCGGAAGAGCUGGTT.

5.2. Molecular docking

Molecular docking was performed using Glide program implemented in Schrödinger package. Crystal structure of CDK2 (PDB code 5NEV) was downloaded from Protein Data Bank (PDB), then protein was optimized by using Protein Preparation Wizard module. Receptor grid file was generated using Receptor Grid Generation module. Compound DC-K2in202 was prepared using LigPrep module to generate protonation states and stereoisomers. Standard precision (SP) mode was adopted in molecular docking, the pose with good hydrogen bond geometries and low energy conformations was considered for further analysis. Docking structures and figures were analyzed and generated based on the PyMOL molecular graphic system.

Author contributions

C.L. and B.Z. directed and supervised the project. T.L. prepared and characterized compounds; J.L. and Y.L. performed biological experiments; T.L., J.L., and P.X. performed computational study; H.J., C.L, and B.Z designed the study. All authors analyzed the data. T.L., J.L., P.X., C.L, and B.Z drafted the manuscript. All authors have given approval to the final version of the manuscript.

Declaration of competing interest

The authors declare that they have no known competing financial interests or personal relationships that could have appeared to influence the work reported in this paper.

Acknowledgements

We are grateful to National Centre for Protein Science Shanghai (Protein Expression and Purification system) for their instrument support and technical assistance. We also gratefully acknowledge the financial supports from the National Natural Science Foundation of China (91853205, 81625022, 81821005to C.L.), K. C. Wong Education to C.L., the Science and Technology Commission of Shanghai Municipality (19XD1404700 and 18431907100 to C.L.) and National Science & Technology Major Project "Key New Drug Creation and Manufacturing Program" (2018ZX09711002-008 to C.L.)

Appendix B. Supplementary data

Supplementary data to this article can be found online at https://doi.org/10.1016/j.ejmech.2021.113281.

References

[1] S. Lim, P. Kaldis, Cdks, cyclins and CKIs: roles beyond cell cycle regulation, Development 140 (2013) 3079–3093.

[2] M. Malumbres, Cyclin-dependent kinases, Genome Biol. 15 (2014) 122.
[3] N. Chunder, L. Wang, C. Chen, W.W. Hancock, A.D. Wells, Cyclin-dependent kinase 2 controls peripheral immune tolerance, J. Immunol. 189 (2012) 5659–5666.
[4] P. Saurus, S. Kuusela, V. Dumont, E. Lehtonen, C.L. Fogarty, M.I. Lassenius, C. Forsblom, M. Lehto, M.A. Saleem, P.H. Groop, S. Lehtonen, Cyclin-dependent kinase 2 protects podocytes from apoptosis, Sci. Rep. 6 (2016), 21664.
[5] F. Granes, M.B. Roig, H.J. Brady, G. Gil-Gomez, Cdk2 activation acts upstream of the mitochondrion during glucocorticoid induced thymocyte apoptosis, Eur. J. Immunol. 34 (2004) 2781–2790.
[6] A.J. Deans, K.K. Khanna, C.J. McNees, C. Mercurio, J. Heierhorst, G.A. McArthur, Cyclin-dependent kinase 2 functions in normal DNA repair and is a therapeutic target in BRCA1-deficient cancers, Cancer Res 66 (2006) 8219–8226.
[7] M. Malumbres, M. Barbacid, Cell cycle, CDKs and cancer: a changing paradigm, Nat. Rev. Canc. 9 (2009) 153–166.
[8] J. Wang, T. Yang, G. Xu, H. Liu, C. Ren, W. Xie, M. Wang, Cyclin-dependent kinase 2 promotes tumor proliferation and induces radio resistance in glioblastoma, Transl Oncol 9 (2016) 548–556.
[9] M. Ying, X. Shao, H. Jing, Y. Liu, X. Qi, J. Cao, Y. Chen, S. Xiang, H. Song, R. Hu, G. Wei, B. Yang, Q. He, Ubiquitin-dependent degradation of CDK2 drives the therapeutic differentiation of AML by targeting PRDX2, Blood 131 (2018) 2698–2711.
[10] X.F. Yin, J. Yu, Y. Zhou, C.Y. Wang, Z.M. Jiao, Z.N. Qian, H. Sun, B.H. Chen, Identification of CDK2 as a novel target in treatment of prostate cancer, Future Oncol. 14 (2018) 709–718.
[11] G. Au-Yeung, F. Lang, W.J. Azar, C. Mitchell, K.E. Jarman, K. Lackovic, D. Aziz, C. Cullinane, R.B. Pearson, L. Mileshkin, D. Rischin, A.M. Karst, R. Drapkin, D. Etemadmoghadam, D.D. Bowtell, Selective targeting of cyclin E1-amplified high-grade serous ovarian cancer by cyclin-dependent kinase 2 and AKT inhibition, Clin. Canc. Res. 23 (2017) 1862–1874.
[12] J.J. Molenaar, M.E. Ebus, D. Geerts, J. Koster, F. Lamers, L.J. Valentijn, E.M. Westerhout, R. Versteega, H.N. Caron, Inactivation of CDK2 is synthetically lethal to MYCN over-expressing cancer cells, Proc. Natl. Acad. Sci. U. S. A. 109 (2009) 12968–12973.
[13] G. Beale, E.J. Haagensen, H.D. Thomas, L.Z. Wang, C.H. Revill, S.L. Payne, B.T. Golding, I.R. Hardcastle, D.R. Newell, R.J. Griffin, C. Cano, Combined PI3K and CDK2 inhibition induces cell death and enhances in vivo antitumour activity in colorectal cancer, Br. J. Canc. 115 (2016) 682–690.
[14] S. Bolin, A. Borgenvik, C.U. Persson, A. Sundstrom, J. Qi, J.E. Bradner, W.A. Weiss, Y.J. Cho, H. Weishaupt, F.J. Swartling, Combined BET bromodomain and CDK2 inhibition in MYC-driven medulloblastoma, Oncogene 37 (2018) 2850–2862.
[15] M.T. Herrera-Abreu, M. Palafox, U. Asghar, M.A. Rivas, R.J. Cutts, I. Garcia-Murillas, A. Pearson, M. Guzman, O. Rodriguez, J. Grueso, M. Bellet, J. Cortes, R. Elliott, S. Pancholi, J. Baselga, M. Dowsett, L.A. Martin, N.C. Turner, V. Serra, Early adaptation and acquired resistance to CDK4/6 inhibition in estrogen receptor-positive breast cancer, Cancer Res 76 (2016) 2301–2313.
[16] A.M. Senderowicz, Flavopiridol: the first cyclin-dependent kinase inhibitor in human clinical trials, Invest. N. Drugs 17 (1999) 313–320.
[17] A. Deep, R.K. Marwaha, M.G. Marwaha, Jyoti, R. Nandal, A.K. Sharma, Flavopiridol as cyclin dependent kinase (CDK) inhibitor: a review, New J. Chem. 42 (2018) 18500–18507.
[18] A.J. Alvi, B. Austen, V.J. Weston, C. Fegan, D. MacCallum, A. Gianella-Borradori, D.P. Lane, M. Hubank, J.E. Powell, W. Wei, A.M. Taylor, P.A. Moss, T. Stankovic, A novel CDK inhibitor, CYC202 (R-roscovitine), overcomes the defect in p53-dependent apoptosis in B-CLL by down-regulation of genes involved in transcription regulation and survival, Blood 105 (2005) 4484–4491.
[19] S.K. Kumar, B. LaPlant, W.J. Chng, J. Zonder, N. Callander, R. Fonseca, B. Fruth, V. Roy, C. Erlichman, A.K. Stewart, C. Mayo, Phase, Dinaciclib, a novel CDK inhibitor, demonstrates encouraging single-agent activity in patients with relapsed multiple myeloma, Blood 125 (2015) 443–448.
[20] D. Parry, T. Guzi, F. Shanahan, N. Davis, D. Prabhavalkar, D. Wiswell, W. Seghezzi, K. Paruch, M.P. Dwyer, R. Doll, A. Nomeir, W. Windsor, T. Fischmann, Y. Wang, M. Oft, T. Chen, P. Kirschmeier, E.M. Lees, Dinaciclib, A novel and potent cyclin-dependent kinase inhibitor, Mol. Canc. Therapeut. 9 (2010) 2344–2353. SCH 727965.
[21] M.D. Seftel, J. Kuruvilla, T. Kouroukis, V. Banerji, G. Fraser, M. Crump, R. Kumar, H.I. Chalchal, M. Salim, R.C. Laister, S. Crocker, S.B. Gibson, M. Toguchi, J.F. Lyons, H. Xu, J. Powers, J. Sederias, L. Seymour, A.E. Hay, The CDK inhibitor AT7519M in patients with relapsed or refractory chronic lymphocytic leukemia (CLL) and mantle cell lymphoma. A Phase II study of the Canadian Cancer Trials Group, Leuk. Lymphoma 58 (2017) 1358–1365.
[22] P.G. Wyatt, A.J. Woodhead, V. Berdini, J.A. Boulstridge, M.G. Carr, D.M. Cross, D.J. Davis, L.A. Devine, T.R. Early, R.E. Feltell, E.J. Lewis, R.L. McMenamin, E.F. Navarro, M.A. O'Brien, M. O'Reilly, M. Reule, G. Saxty, L.C. Seavers, D.M. Smith, M.S. Squires, G. Trewartha, M.T. Walker, A.J. Woolford, Identification of N-(4-piperidinyl)-4-(2,6-dichlorobenzoylamino)-1H-pyrazole-3-carboxamide (AT7519), a novel cyclin dependent kinase inhibitor using fragment-based X-ray crystallography and structure based drug design, J. Med. Chem. 51 (2008) 4986–4999.
[23] B.C. Cho, G.K. Dy, R. Govindan, D.W. Kim, N.A. Pennell, G. Zalcman, B. Besse, J.H. Kim, G. Koca, P. Rajagopalan, S. Langer, M. Ocker, H. Nogai, F. Barlesi, Phase Ib/II study of the pan-cyclin-dependent kinase inhibitor roniciclib in combination with chemotherapy in patients with extensive-disease small-cell lung cancer, Lung Canc. 123 (2018) 14–21.
[24] U. Lücking, R. Jautelat, M. Krüger, T. Brumby, P. Lienau, M. Schäfer, H. Briem, J. Schulze, A. Hillisch, A. Reichel, A.M. Wengner, G. Siemeister, The lab oddity prevails: discovery of pan-CDK inhibitor (R)-S-cyclopropyl-S-(4-{[4-{[(1R,2R)-2-hydroxy-1-methylpropyl]oxy}-5-(trifluoromethyl)pyrimidin-2-yl]amino}phenyl)sulfoximide (BAY ;1000394) for the treatment of cancer, ChemMedChem 8 (2013) 1067–1085.
[25] A. Degrassi, M. Russo, C. Nanni, V. Patton, R. Alzani, A.M. Giusti, S. Fanti, M. Ciomei, E. Pesenti, G. Texido, Efficacy of PHA-848125, a cyclin-dependent kinase inhibitor, on the K-Ras(G12D)LA2 lung adenocarcinoma transgenic mouse model: evaluation by multimodality imaging, Mol. Canc. Therapeut. 9 (2010) 673–681.
[26] M.G. Brasca, N. Amboldi, D. Ballinari, A. Cameron, E. Casale, G. Cervi, M. Colombo, F. Colotta, V. Croci, R. D'Alessio, F. Fiorentini, A. Isacchi, C. Mercurio, W. Moretti, A. Panzeri, W. Pastori, P. Pevarello, F. Quartieri, F. Roletto, G. Traquandi, P. Vianello, A. Vulpetti, M. Ciomei, Identification of N,1,4,4-tetramethyl-8-{[4-(4-methylpiperazin-1-yl)phenyl]amino}-4,5-dihydro-1H-py razolo[4,3-h]quinazoline-3-carboxamide (PHA-848125), a potent, orally available cyclin dependent kinase inhibitor, J. Med. Chem. 52 (2009) 5152–5163.
[27] M.V. Reddy, B. Akula, S.C. Cosenza, S. Athuluridivakar, M.R. Mallireddigari, V.R. Pallela, V.K. Billa, D.R. Subbaiah, E.V. Bharathi, R. Vasquez-Del Carpio, A. Padgaonkar, S.J. Baker, E.P. Reddy, Discovery of 8-cyclopentyl-2-[4-(4-methyl-piperazin-1-yl)-phenylamino]-7-oxo-7,8-dihydro-pyrid o[2,3-d]pyrimidine-6-carbonitrile (7x) as a potent inhibitor of cyclin-dependent kinase 4 (CDK4) and AMPK-related kinase 5 (ARK5), J. Med. Chem. 57 (2014) 578–599.
[28] R. Jorda, D. Hendrychova, J. Voller, E. Reznickova, T. Gucky, V. Krystof, How selective are pharmacological inhibitors of cell-cycle-regulating cyclin-dependent kinases? J. Med. Chem. 61 (2018) 9105–9120.
[29] A.S. Clark, T.B. Karasic, A. DeMichele, D.J. Vaughn, M. O'Hara, R. Perini, P. Zhang, P. Lal, M. Feldman, M. Gallagher, P.J. O'Dwyer, Palbociclib (PD0332991)-a selective and potent cyclin-dependent kinase inhibitor: a review of pharmacodynamics and clinical development, JAMA Oncol 2 (2016) 253–260.
[30] J.W. Goldman, P. Shi, M. Reck, L. Paz-Ares, A. Koustenis, K.C. Hurt, Treatment rationale and study design for the juniper study: a randomized phase III study of Abemaciclib with best supportive care versus erlotinib with best supportive care in patients with stage IV non-small-cell lung cancer with a detectable KRAS mutation whose disease has progressed after platinum-based chemotherapy, Clin. Lung Canc. 17 (2016) 80–84.
[31] Y.Y. Syed, Ribociclib: first global approval, Drugs 77 (2017) 799–807.
[32] C.R. Coxon, E. Anscombe, S.J. Harnor, M.P. Martin, B. Carbain, B.T. Golding, I.R. Hardcastle, L.K. Harlow, S. Korolchuk, C.J. Matheson, D.R. Newell, M.E. Noble, M. Sivaprakasam, S.J. Tudhope, D.M. Turner, L.Z. Wang, S.R. Wedge, C. Wong, R.J. Griffin, J.A. Endicott, C. Cano, Cyclin-dependent kinase (CDK) inhibitors: structure-activity relationships and insights into the CDK-2 selectivity of 6-substituted 2-arylaminopurines, J. Med. Chem. 60 (2017) 1746–1767.
[33] W. Cheng, Z. Yang, S. Wang, Y. Li, H. Wei, X. Tian, Q. Kan, Recent development of CDK inhibitors: an overview of CDK/inhibitor co-crystal structures, Eur. J. Med. Chem. 164 (2019) 615–639.
[34] M.S. Squires, R.E. Feltell, N.G. Wallis, E.J. Lewis, D.M. Smith, D.M. Cross, J.F. Lyons, N.T. Thompson, Biological characterization of AT7519, a small-molecule inhibitor of cyclin-dependent kinases, in human tumor cell lines, Mol. Canc. Therapeut. 8 (2009) 324–332.
[35] L. Cheng, F. Rossi, W. Fang, T. Mori, D. Cobrinik, Cdk2-dependent phosphorylation and functional inactivation of the pRB-related p130 protein in pRB(-), p16INK4A(+) tumor cells, J. Biol. Chem. 275 (2000) 30317–30325.
[36] D.J. Wood, S. Korolchuk, N.J. Tatum, L.Z. Wang, J.A. Endicott, M.E.M. Noble, M.P. Martin, Differences in the conformational energy landscape of CDK1 and CDK2 suggest a mechanism for achieving selective CDK inhibition, Cell Chem Biol 26 (2019) 121–130 e125.
[37] M. Kitagawa, H. Higashi, H.K. Jung, I. SuzukiTakahashi, M. Ikeda, K. Tamai, J. Kato, K. Segawa, E. Yoshida, S. Nishimura, Y. Taya, The consensus motif for phosphorylation by cyclin D1-Cdk4 is different from that for phosphorylation by cyclin A/E-Cdk2, EMBO J. 15 (1996) 7060–7069.
[38] G.S. Choudhary, S. Al-Harbi, S. Mazumder, B.T. Hill, M.R. Smith, J. Bodo, E.D. Hsi, A. Almasan, MCL-1 and BCL-xL-dependent resistance to the BCL-2 inhibitor ABT-199 can be overcome by preventing PI3K/AKT/mTOR activation in lymphoid malignancies, Cell Death Dis. 6 (2015) e1593.
[39] A. Sancar, L.A. Lindsey-Boltz, K. Unsal-Kacmaz, S. Linn, Molecular mechanisms of mammalian DNA repair and the DNA damage checkpoints, Annu. Rev. Biochem. 73 (2004) 39–85.